Helsinki University of Technology
Department of Chemical Technology
Laboratory of Physical Chemistry and Electrochemistry
Espoo 2004

Chemical Thermodynamics of Aqueous Electrolyte Systems for Industrial and Environmental Applications

Justin Salminen

TEKNILLINEN KORKEAKOULU
TEKNISKA HÖGSKOLAN
HELSINKI UNIVERSITY OF TECHNOLOGY
UNIVERSITE DE TECHNOLOGIE D'HELSINKI

Chemical Thermodynamics of Aqueous Electrolyte Systems for Industrial and Environmental Applications

Justin Salminen

ABSTRACT

This thesis consists of studies of chemical thermodynamics of aqueous electrolytes for industrial and environmental applications. Calculations have been used to represent vapor-liquid-solid equilibria and chemical equilibria for aqueous systems including solubility of gases. Modern simulation methods combined with experiments provide a useful tool for the research and design of new processes as well as evaluating changes in the operational conditions of chemical processes. The Gibbs energy minimization methods ChemSage, and ChemSheet have been used along with activity coefficient models including Pitzer ion interaction model. The calculated results were compared if possible with experiments or with reference data. Further this work consists of studies on oxygen-pressurized peroxide bleaching, which is an important sequence of total chlorine free (TCF) bleaching for environmental reasons. The solution properties like pH have been measured and modelled both in pure H_2O_2-NaOH-H_2O system and in bleaching conditions. Further, the thermodynamic multicomponent model was used with kinetic constraints for pH calculations in reactive solution. The knowledge of the pulp- and solution properties along with the results of the model calculations could be used for optimisation of the bleaching process with respect to reaction time and temperature. Thermodynamics provides a practical tool for the estimation of the chemical states of pulp and paper solutions as well as in hydrometallurgical applications. Such a fundamental approach relates to the chemical energy, chemical reactions, solubility of gases and salts, and an important online process parameter pH. The Gibbs energy approach was further applied to equilibrium and reaction dynamic studies of multiphase CO_2-$CaCO_3$-H_2O system.

PREFACE

Helsinki, December 2003

Justin Salminen

CONTENTS

LIST OF PUBLICATIONS

I.   J. Salminen, P. Koukkari, J. Jäkärä, and A. Paren, Thermochemical Experiments and Modelling of the PO-Bleaching Stage, JPPS. **26** (12), 441-447 (2000).

II. T. Kaskiala and J. Salminen, Oxygen Solubility in Industrial Process Development, Ind Eng. Chem. Res. **42**, 1827-1831 (2003).

III. J. Salminen and O. Antson, Physico-Chemical Modelling of Bleaching Solution and Reaction, Ind. Eng. Chem. Res. **41**, 3312-3316 (2002).

IV. P. Koukkari, R. Pajarre, H. Pakarinen, and J. Salminen, Practical Multiphase Models for Aqueous Process Solutions, Ind. Eng. Chem. Res. **40**, 5014-5020 (2001).

V.   J. Salminen, P. Kobylin, O. Chiavone-Filho, and S. Liukkonen, Gibbs Energy Approach for Aqueous Processes with HF, HNO_3 and CO_2-$CaCO_3$, accepted, to be published in AIChE J. **50** No. 6, (2004).

STATEMENT ON THE AUTHOR'S ROLE IN LISTED PUBLICATIONS

Statement about the role of Justin Salminen in the five publications included in his thesis

Justin Salminen has been the corresponding author in all the Papers I-V. He has had an active role in planning the experiments-, and modelling, as well as in representation of the results, except for those presented in Figures 4 and 5 in the Paper I and Figures 6 and 7 in the Paper II. In addition, he was responsible for writing up the papers I-V. In the paper IV Justin Salminen had active role on planning the experimental set up, supervising the experiments, writing up the paper together with other authors.

In addition to the Papers I-V, this thesis includes some unpublished results in area of the thesis study.

Espoo, 2 December 2003

Simo Liukkonen
Professor

1. INTRODUCTION

Chemical thermodynamics focuses on energy changes in chemical reactions and provides a fundamental and widely applicable tool for studying multiphase solutions in aqueous electrolyte systems. Chemical equilibrium shows the natural boundaries of the physical and chemical interactions as contributors in different chemical environments, temperatures and pressures. Thermodynamics answers the question by how much, and in what direction, the system responds to the changes. It practically relates the changes in chemical energy to measurable parameters including pressure, temperature, compositions, solubilities and pH. The knowledge of both physical and chemical equilibrium including reactions is essential. Electrolytes are often present in real industrial processes naturally or as added separation agents. Ions have a unique effect on the non-ideal behaviour in water solutions and models that can treat electrolyte solutions in wide concentration ranges at different temperatures and pressures along with computer aided calculation routine are needed. When data is available, modern computer-aided calculation methods provide together with laboratory experiments, pilot- and mill- scale experience useful and practical solutions for treating industrial and environmental processes.

2. THERMODYNAMIC PRINCIPLES

2.1 Internal energy

The first law of thermodynamics states that internal energy U of the system is a sum of heat q and work w.

$$U = q + w \qquad (2.1)$$

One cannot measure the absolute values of internal energy, thus only the changes are measurable. For the infinitesimal change in state one obtains

$$dU = dq + dw \qquad (2.2)$$

The differentials of heat and work dq and dw are inexact differentials and the integrals of these quantities depend on the path chosen. The internal energy is a state function and depends only on the initial and the final state. The entropy S is defined by the exchange of heat quantity in a reversible process divided by absolute temperature.

$$dS = \frac{dq_{rev}}{T} \qquad (2.3)$$

From the first law of thermodynamics one obtains the relation between entropy, internal energy and the volumetric displacement work.

$$dS = \frac{dU - dw}{T} = \frac{dU + PdV}{T} \qquad (2.4)$$

where

$$dU = TdS - PdV \qquad (2.5)$$

In systems where chemical reactions occur, there are additional independent variables, the chemical amounts n_i of the components present.[1,2] The internal energy is a function of S, V and n_i's of the system $U = U(S, V, n_i, \ldots, n_k)$. The total differentiation yields

$$dU = \left(\frac{\partial U}{\partial S}\right)_{V,n_i} dS + \left(\frac{\partial U}{\partial V}\right)_{S,n_i} dV + \sum_i \left(\frac{\partial U}{\partial n_i}\right)_{S,V,n_j} dn_i \qquad (2.6)$$

The coefficients for the partial derivatives in the previous equation are defined as temperature T, negative to pressure $-P$ and chemical potential μ_i. It then follows that

$$dU = TdS - PdV + \sum_i \mu_i dn_i \qquad (2.7)$$

By performing the Legendre transformation for internal energy $U(S,V,n_i,\ldots,n_k)$ one obtains other thermodynamic potential functions by means of a different sets of thermodynamic variables. The potential functions of enthalpy $H(S,P,n_i,\ldots,n_k)$, Helmholtz energy $A(T,V,n_i,\ldots,n_k)$, and Gibbs energy $G(T,P,n_i,\ldots,n_k)$ are then obtained.[3]

$$dH = TdS + VdP + \sum_i \mu_i dn_i \qquad (2.8)$$

$$dA = -SdT - PdV + \sum_i \mu_i dn_i \qquad (2.9)$$

$$dG = -SdT + VdP + \sum_i \mu_i dn_i \qquad (2.10)$$

where

$$\mu_i \equiv \left(\frac{\partial U}{\partial n_i}\right)_{S,V,n_j} = \left(\frac{\partial H}{\partial n_i}\right)_{S,P,n_j} = \left(\frac{\partial A}{\partial n_i}\right)_{T,V,n_j} = \left(\frac{\partial G}{\partial n_i}\right)_{T,P,n_j} \qquad (2.11)$$

Chemical potential μ_i show how the thermodynamic potential function changes when material is added or removed in the system.

2.2 Entropy in a reactive system

Entropy can be divided into two parts entropy flow and entropy production.[4] The differential change of entropy is then expressed as

$$dS = d_E S + d_I S \qquad (2.12)$$

$d_E S$ is the entropy change due to the exchange of energy and matter (entropy flow), and $d_I S$ is the entropy change due to irreversible processes within the system (entropy production). For a system where a chemical reaction occurs the infinitesimal change of internal energy can be written as

$$dU = Td_E S + Td_I S - PdV + \sum_i \mu_i dn_i \qquad (2.13)$$

Arranging the previous equation one obtains a fundamental equation

$$dS = d_E S + d_I S = \frac{dU + PdV}{T} - \frac{1}{T}\sum_i \mu_i dn_i \qquad (2.14)$$

where

$$d_I S = -\frac{1}{T}\sum_i \mu_i dn_i \qquad (2.15)$$

2.3 Gibbs energy in a reactive system

For the Gibbs energy change at constant T and P in a single phase is

$$dG = \sum_i \mu_i dn_i \tag{2.16}$$

In chemically reactive systems, the change of chemical amounts dn_i can be expressed as $dn_i = v_i d\xi$, where v_i is the stoichiometric number of the species in the reaction and ξ is the extent of the reaction in moles.

$$\left(\frac{\partial G}{\partial \xi}\right)_{T,P} = \sum_i v_i \mu_i \tag{2.17}$$

The values of the stoichiometric coefficients are positive ($v_i>0$) for products and negative ($v_i<0$) for reactants. At equilibrium, the Gibbs energy is at the minimum, which corresponds to a zero slope in the two-dimensional phase space, and the right-hand side of equation (2.18) is zero. Writing the chemical potential by means of standard state chemical potentials and activities gives

$$\left(\frac{\partial G}{\partial \xi}\right)_{T,P} = \sum_i v_i \mu_i = \sum_i v_i \mu_i^\circ + RT \sum_i v_i \ln a_i = 0 \tag{2.18}$$

$$\sum_i v_i \mu_i^\circ = -RT \sum_i \ln a_i^{v_i} = -RT \ln \prod_i a_i^{v_i} \tag{2.19}$$

The thermodynamic equilibrium constant K is defined by means of the product of activities a that is related to the standard molar Gibbs energy of a reaction $\Delta_r G_m^\circ$.

$$K = \prod_i a_i^{v_i} \tag{2.20}$$

$$\Delta_r G_m^\circ = -RT \ln K \tag{2.21}$$

The extensive quantity of Gibbs energy of the system is obtained as a sum of the chemical potentials multiplied by their chemical amounts over all the species and phases.

$$G = \sum_\alpha \sum_i n_i^\alpha \mu_i^\alpha \tag{2.22}$$

In the case where there exist one gas phase α, one liquid phase β and invariant pure solid phases κ_i one can write

$$G = G^{\alpha}(T,P,n_i^{\alpha},...,n_j^{\alpha}) + G^{\beta}(T,P,n_i^{\beta},...,n_j^{\beta}) + G^{\kappa_1}(T,P,n_{S_1}^{\kappa_1})$$
$$+...+G^{\kappa_n}(T,P,n_{S_n}^{\kappa_n})$$

(2.23)

The total Gibbs energy of a system is constructed by writing the chemical potential or the partial molar Gibbs energy μ_i for each species. The total Gibbs energy G^{α} of a gas phase is the sum of all the components in the gas phase

$$G^{\alpha} = \sum_{n=1} n_n \left(\mu_n^{\circ} + RT \ln\left(\frac{y_n \phi_n P}{P^{\circ}} \right) \right)$$

(2.24)

The total Gibbs energy G^{β} of an aqueous liquid phase is the sum of the Gibbs energies of water, dissolved, salts and dissolved gases:

$$G^{\beta} = n_w \left(\mu_w^{\circ} + RT \ln(x_w \gamma_w^x) \right) + \sum_{i=1} n_i \left(\mu_i^{\ominus} + RT \ln\left(\frac{m_i \gamma_i^m}{m^{\circ}} \right) \right)$$
$$+ \sum_{n=1} n_n \left(\mu_n^{\ominus} + RT \ln\left(\frac{m_n \gamma_n^m}{m^{\circ}} \right) \right)$$

(2.25)

The total Gibbs energy G^{κ} of the solid phases is

$$G^{\kappa} = \sum_{\kappa=1} n_{\kappa} \mu_{\kappa}^{\circ}$$

(2.26)

2.4. Gibbs energy approach for the calculations

The total Gibbs energy of a system is constructed by writing the chemical potential μ_i for each species. The chemical potentials of pure species are derived through the tabulated values of the enthalpy of formation, heat capacity and the absolute entropy.

$$H_i^{\circ}(T) = \Delta_f H_i^{\circ}(298.15\,\mathrm{K}) + \int_{298.15\mathrm{K}}^{T} C_P(T)\,\mathrm{d}T + \sum (\Delta_t H)$$

(2.27)

$$S_i^{\circ}(T) = S_i^{\circ}(298.15\,\mathrm{K}) + \int_{298.15\mathrm{K}}^{T} \left(\frac{C_P(T)}{T} \right)\mathrm{d}T + \sum \left(\frac{\Delta_t H}{T_t} \right)$$

(2.28)

where C_P is the temperature-dependent heat capacity function, $\Delta_t H$ is the heat of transition at the transition temperature at standard pressure 1 bar. The standard molar Gibbs energies of a species i for pure species are then obtained

$$G_{m,i}^{\circ}(T) = H_i^{\circ}(T) - TS_i^{\circ}(T) \qquad (2.29)$$

where the standard chemical potential $\mu_i^{\circ}(T)$ of the pure species i is set equal to $G_{m,i}^{\circ}(T)$ at standard pressure 1 bar at temperature T. The total Gibbs energy, G, of a system seeks into its minimum through chemical reactions by minimizing equation (2.22).

H, S and C-data, T and P
Chemical amounts
Electroneutrality condition $\longrightarrow$ **min(G)** $\longrightarrow$
Material constrains

Chemical equilibrium
Physical equilibrium
Fugacities, activities
Dynamic chemical state
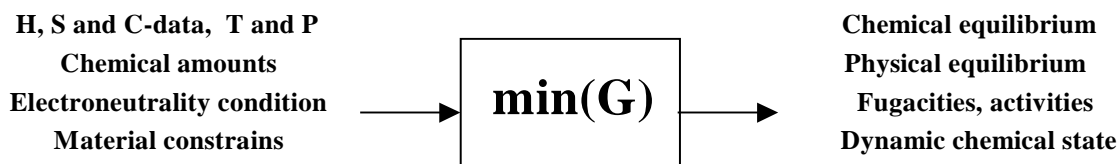
Figure 2-1. The calculation procedure for aqueous multicomponent solutions with Gibbs energy approach.

The Gibbs energy minimization routine yields the solubilities as well as the chemical speciation in the aqueous phase. Temperature-dependent activity coefficient models are combined and used together with well-established multicomponent Gibbs free-energy minimization routines like Chemsheet® and Chemsage®.[5-8] Chemsheet® enables one to formulate and run one's multiphase process chemistry to and from a spreadsheet in MS-Excel. One can produce active simulation workbooks for practical engineering needs. The use of ChemSheet is schematically shown for $NaOH$-H_2O_2-O_2-H_2O system in figure 2-2.
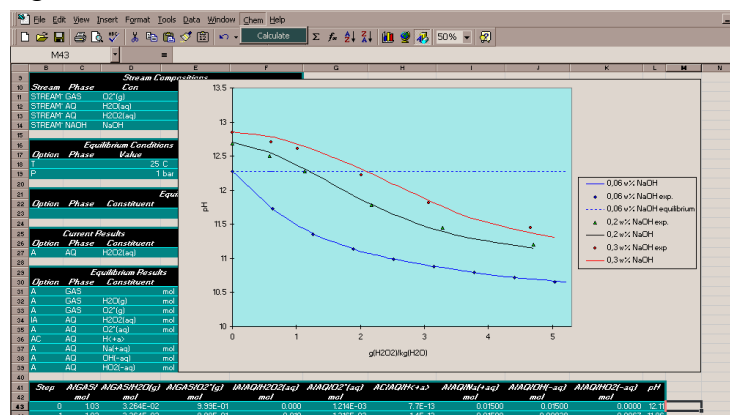
Figure 2-2. ChemSheet® works as an add-in of general thermodynamics to an MS-Excel-spreadsheet. Thus, the tabulated data is combined with worksheet calculation techniques in a practical fashion. The frame shows Chemsheet calculation environment.

3. CHEMICAL EQUILIBRIUM IN AQUEOUS MEDIA

3.1. Thermodynamics of gas solubility

Dissolved gases are commonly used as reactive chemical agents in processes in atmospheric conditions as well as at elevated pressures. The gas solubility phenomena are important in many industrial as well as environmental applications. In this work the experiments and modelling results have been applied in metallurgical and pulp and paper processes. The processes are commonly controlled by the partial pressure of the reactive gas, temperature and chemical composition of the reactive solution. Theory, measurements and simulations together provide sufficient information for practical applications. For an ideal gas component in an ideal mixture the chemical potential is expressed by means of standard chemical potential $\mu_n^{\circ V}(T)$ and the logarithm term that includes the fugacity $f_n = y_n \phi_n P$ of the gas n.

$$\mu_n^V(T,P,y_n) = \mu_n^{\circ V}(T) + RT \ln\left(\frac{f_n}{P^{\circ}}\right) \tag{3.1}$$

The numeric values of chemical potentials in mixtures are expressed by a standard term and logarithmic activity term. The chemical compositions of individual species in the condensed mixture phases are usually described in three different concentration units like mole fraction x_i, molality m_i and concentration c_i. The absolute value of the chemical potential μ_i does not change regardless of what scale is used but the standard state value is different in different scales, as also is the activity term of the solute components. In non-ideal mixtures, the logarithmic composition factor of the chemical potential is expressed by the activity term $a_n = \gamma_n x_n$.

$$\mu_n^L(T,P,x_n) = \mu_n^{\ominus L}(T,P) + RT \ln a_n \tag{3.2}$$

At equilibrium between the vapour and liquid phases the chemical potentials are equal

$$\mu_n^V = \mu_n^L \tag{3.3}$$

The chemical potential change $\Delta\mu_n^{\circ}$ for a gas in the dissolution process at standard state then becomes

$$\Delta\mu_n^{\circ}(T,P) = \mu_n^{\ominus L} - \mu_n^{\circ V} = RT \ln\left(\frac{y_n \phi_n P}{x_n \gamma_n P^{\circ}}\right) \tag{3.4}$$

The standard chemical potential of the dissolved component $\mu_n^{\ominus L}(T,P)$ in the liquid phase is hypothetical. The hypothetical state refers to an extrapolation along the Henry's law slope from the infinite dilution of volatile component n to its mole

fraction $x_n = 1$. The standard state chemical potential for a gas component is only a function of temperature, while for the liquid phase the components are functions of temperature and pressure. If the gas is assumed ideal at pressure p_n and the liquid phase is assumed ideal, the fugacity coefficient has numerical value $\phi_n = 1$ and the activity coefficient $\gamma_n = 1$ in dilute solution. In Figure 3-1, the standard chemical potential change $\Delta\mu_n^\circ$ for oxygen dissolved in water is shown within 293-323 K. The calculated results were verified with measurements by Morrison–Billett gas solubility apparatus and reference data.
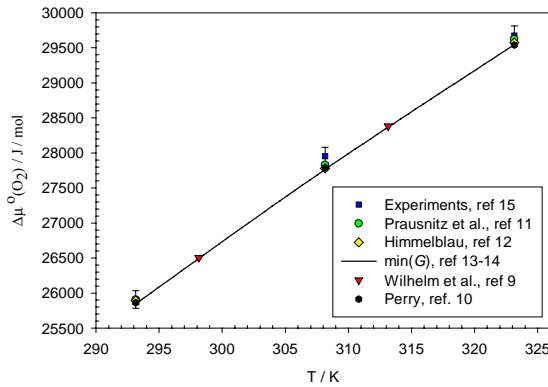
Figure 3-1. Temperature dependence for standard chemical potential change in solution process for oxygen in pure water.[9-15]

The calculated standard chemical potential data values at 293, 308 and 323 K shown in Figure 3-1 yield 0.7- 1.0 % average absolute deviation (AAD%) compared to other reference data solubilities.[10-12] The average absolute deviation, AAD % from average solubility values is given by the following equation:

$$\text{AAD}\% = \frac{100}{n} \sum_{i=1}^{n} \left| \frac{m_{\text{ave,i}}^{\text{s}} - m_{\text{calc,i}}^{\text{s}}}{m_{\text{ave,i}}^{\text{s}}} \right| \tag{3.5}$$

where $m_{\text{ave}}^{\text{s}}$ is the average solubility value of all data points from each data point in[10-12] and $m_{\text{calc}}^{\text{s}}$ is the individual solubility value calculated by the model. At standard state pressure 1 bar the relation between Henry's law constant and chemical potential change becomes

$$k_H(T)/\text{bar} = \exp\left(\Delta\mu_n^\circ/RT\right) \tag{3.6}$$

Henry's law constant k_H is a strong function of temperature but to a lesser degree a function of the pressure. The partial derivative of k_H with respect of temperature at constant pressure yields

$$\left(\frac{\partial \ln k_H}{\partial T}\right)_P = \frac{\partial}{R\partial T}\left(\frac{\Delta \mu_n^\circ}{T}\right)_P = -\frac{H_{m,n}^{\ominus L} - H_{m,n}^{\circ V}}{RT^2} = -\frac{\Delta H_{m,n}^\circ}{RT^2} \tag{3.7}$$

$H_{m,n}^{\circ V}$ is the standard molar enthalpy of the gas component n in the gas phase. $H_{m,n}^{\ominus L}$ is the standard partial molar enthalpy of the dissolved gas at infinite dilution. $\Delta H_{m,n}^\circ$ is the standard enthalpy change of the solution in the dissolution process of a gas n. At the minimum solubility and maximum point of k_H the sign of the dissolution enthalpy $\Delta H_{m,n}^\circ$ changes. A wide selection of reference- data sets and temperature-dependent correlations are available for oxygen solubility in water and Henry's law constant.[9-25] Henry's constant increases with temperature, passes through a maximum, and then declines at higher temperatures. The pressure dependence of Henry's law constant is obtained through differentiation of the chemical potential with respect to pressure at constant temperature.

$$\left(\frac{\partial \ln k_H}{\partial P}\right)_T = \frac{1}{RT}\left(\frac{\partial (\Delta \mu_n^\circ)}{\partial P}\right)_T = \frac{1}{RT}\left(\frac{\partial \left[\mu_n^{\ominus L}(T,P) - \mu_n^{\circ V}(T)\right]}{\partial P}\right)_T \tag{3.8}$$

The partial derivative of standard chemical potential in the vapour phase with respect to pressure is zero. For a dissolved gas, it is the partial molar volume $V_{m,n}^\infty$ of the dissolved gas n at infinite dilution in a solvent.

$$\left(\frac{\partial \ln k_H}{\partial P}\right)_T = \frac{1}{RT}\left(\frac{\partial \mu_n^{\ominus L}}{\partial P}\right)_T = \frac{V_{m,n}^\infty}{RT} \tag{3.9}$$

In Table 3-1, various data points are shown for Henry's law constants k_H for oxygen solubility in pure water. These include calculated values and experimental results with moderate pressure Morrison-Billett apparatus.[15,16]

Table 3-1. Henry's law constants k_H for oxygen solubility in pure water obtained from reference data, Gibbs energy calculations and by moderate pressure Morrison-Billett apparatus.[15-17]

T /°C	k_H / bar[10]	k_H / bar[11]	k_H / bar[12]	k_H / bar[min(G), 13,14]	k_H / bar[15]
20	40630	41289	41105	40312	41350
35	51372	52216	51183	50880	54770
50	59580	61453	60326	59688	62670

The experimental procedure with Morrison-Billett gas solubility apparatus is described here briefly. The facility was tested with oxygen, nitrogen and hydrogen solubility in

pure water for further use with industrially interesting aqueous mixed solvents. The apparatus was designed for measurements in the range of 1.5- 6 bar total pressure. All the pressure and temperature sensors were calibrated. In the experiments, the apparatus was set to the desired temperature and pressure. The temperature could be set within $0.1^{\circ}C$ accuracy. Degassed water was then pumped into the absorption spiral in order to obtain saturation between the gas and liquid. Two chambers, the absorption and the equilibrium chamber, were connected with a u-tube and between them there was a horizontal connecting pipe with a valve. The stationary state was obtained when the amount of collected saturated water at the bottom of the u–tube was equal to the amount of pumped water. The middle valve was then closed. After a typically 2-hour measurement time, the middle valve was opened and the change of water level between the two tubes was defined by hydrostatic pressure. The gas solubility values could then be obtained by measuring the amount in grams of collected saturated solvent and the volume difference. The measured solubility values were found to be systematically lower than given by Henry's law. The accuracy of the facility depended mainly on the degassing of the water and 1- 3 mbar pressure decrease in the equilibrium chamber during the measurement. These factors both lower the measured solubility value. On the other hand, the pressure dependency at each temperature was found linear with an average correlation of $R^2 = 0.9996$ for oxygen, nitrogen and hydrogen gases. The total accuracy of the apparatus was defined to be ± 5 % including a ± 1 % error factor related to controlling the total pressure, temperature gradients and the evaporation of the collected saturated solvent. The modified Morrison-Billett apparatus was considered satisfactory for evaluating the gas solubility at moderate pressures. In Figure 3-2, the solubility of oxygen is shown at 80-120°C and 10-30 bar oxygen partial pressures. The Gibbs energy minimization results are verified with reference data.
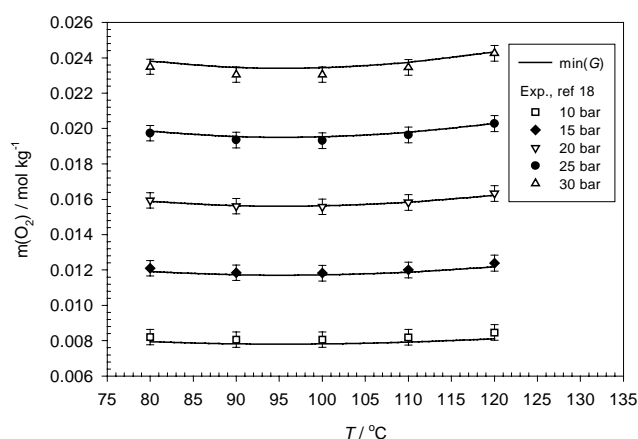

Figure 3-2. Oxygen solubility in pure water at elevated pressures between 80 and 120°C. The model results are compared with the experiments.[18]

3.2 Salt effects

The addition of salt to water changes its solvent properties. It can reduce or increase the solubility of gas. This phenomenon is commonly called the salting in and out effect. The chemical potential for a gas, which has been dissolved in pure water, is

$$\mu_n = \mu_n^\ominus + RT \ln \gamma_n^\circ x_n^\circ \tag{3.10}$$

where γ_n° is the activity coefficient of the gas dissolved in pure water and x_n° is the solubility of the gas in pure water in mole fraction. The chemical potential μ_n for a gas dissolved in electrolyte solution is:

$$\mu_n = \mu_n^\ominus + RT \ln \gamma_n x_n \tag{3.11}$$

where γ_n is the activity coefficient of dissolved gas in electrolyte solution and x_n is the solubility of the gas in electrolyte solution in mole fraction unit. The change in Gibbs free energy becomes

$$\Delta \mu_n = RT \ln \frac{\gamma_n x_n}{\gamma_n^\circ x_n^\circ} \tag{3.12}$$

Setschenow noticed that in dilute solutions the logarithm of the activity coefficient of the gas is a linearly dependent function of the molality of the dissociated salt.[26]

$$\log \gamma_n = K_{n,MX} m_{MX} \tag{3.13}$$

where $K_{n,MX}$ is the salting out coefficient in [kg mol^{-1}] and m_{MX} is the molality of the electrolyte in [mol kg^{-1}]. The slope of the line depends on the gas, the solvent and the salt. At higher salt molalities, the relationship becomes non-linear. Setting chemical potentials of the gas in the gas phase and in the liquid phase equal in the pure solvent and in the salt solutions, one obtains a relation that can be related to the with Setschenow equation.[26-28]

$$\ln\left(\frac{x_n^\circ}{x_n}\right) = \ln\left(\frac{m_n^\circ}{m_m}\right) = \ln\left(\frac{\gamma_n}{\gamma_n^\circ}\right) + \int_{P_{solvent}^*}^{P} \frac{\left(V_{m,n} - V_{m,n}^\infty\right)}{RT} dP = k_{n,MX} m_{MX} \tag{3.14}$$

At low or moderate pressures the contribution of the integral is small and can be ignored. The symbols γ_i°, x_i° and $k_{n,MX}$ refer to the system with salt molality $m_{MX} = 0$. Also one should note that

$$K_{n,MX} = 2k_{n,MX} / 2.303 \tag{3.15}$$

The oxygen solubility measurements and calculations in pure water and in sulphuric acid solutions at atmospheric pressure are shown in Figure 3-3. The salting out of oxygen is clearly observed.
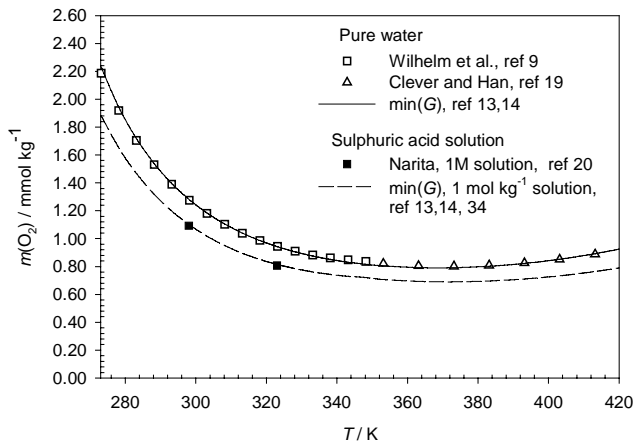
Figure 3-3. Experimental and calculated values of oxygen solubility in pure water and in sulphuric acid solution at 1 atm oxygen partial pressure. The calculated values shown as a dotted line represent $m(H_2SO_4)=1$ mol kg^{-1} solution.

In Figure 3-3, the average deviation of the calculated values for pure water was found at 0.88 % and the maximum at 2.0 % within 273.15- 430 K. At a constant temperature, the addition of sulphuric acid decreases the oxygen solubility as shown by the experiments and model results. According to the literature, the salting out of oxygen is linear up to 1.5 mol dm^{-3} sulphuric acid solutions.[29] There exist little data on the equilibrium and kinetics of oxygen solubility in reactive sulphuric acid solutions.[30-33] The knowledge of the solubility of gases in acidic solutions is a relevant step for studying the leaching process for example. In Figure 3-4, the dissolution kinetics of oxygen is shown. These measurements were carried out in an agitated vessel using a commonly used dynamic pressure method.[31] The response time of the analyser is a few seconds, which compared to the slow dissolution process was considered satisfactory. The time-dependent increase of the solubility of oxygen was taken into account in the thermodynamic model by increasing the oxygen pressure exposed to a volume element according to measured dissolution in pure water. The sulphuric acid-oxygen interaction was included to this empirically determined solubility curve result decrease of solubility throughout the time dependent curve measured.[34,35]

Figure 3-4. The experimental[31] and calculated dissolution kinetics of oxygen in pure water and in 1 mol kg^{-1} sulphuric acid solution at 40°C.
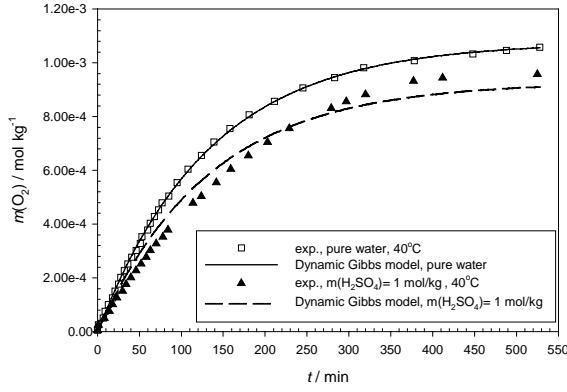
3.3 Dilute electrolyte solutions

Debye and Hückel introduced a quantitative representation of the distribution of ions in an electrolyte solution.[36] They used a model of complete ionization to rigid spherically symmetrical ions in a continuous medium with the macroscopic permittivity of the solvent. In their model, a central ion was chosen. An average electrostatic potential ψ as a function of distance from the central ion was assumed to obey the Poisson-Boltzmann differential equation. In other words, the assumption was that all the deviations from the ideal solution could be described entirely by electrostatic long-range forces between the ions. The interactions between the ions and solvent molecules were ignored. The mean activity coefficient for an electrolyte in water is obtained as an analytical solution of the second order Poisson-Boltzmann differential equation. It yields an expression of the Helmholtz energy difference in the charging process. The differentiation of the electrostatic Helmholtz energy yields the mean activity coefficient of an electrolyte in water,

$$\ln \gamma_{\pm} = -\frac{3A_{\phi}|z_+ z_-|\sqrt{I}}{1+ba\sqrt{I}} \tag{3.16}$$

$$A_{\phi} = \frac{1}{3}\sqrt{2\pi N_A \rho_w}\left(\frac{e^2}{4\pi\varepsilon_o\varepsilon_r kT}\right)^{3/2} \tag{3.17}$$

$$b = \sqrt{\frac{8\pi e^2 N_A \rho_w}{\varepsilon_r kT}} \tag{3.18}$$

where: A_{ϕ} is osmotic Debye and Hückel parameter

                N_A Avogadro's number = $6.023 \cdot 10^{23}$

                ρ_w density of the solvent, [kg m^{-3}]

                ε_0 permittivity of vacuum

                ε_r relative permittivity

                e electronic charge = $1.602 \cdot 10^{-19}$ C

                k Boltzmann's constant = $1.38 \cdot 10^{-23}$ J K^{-1}

The parameter a is the distance of the closest approach between two ions. It is used as an adjustable parameter. The ionic strength I is defined as follows where z_i is the charge number of the i: th particle

$$I = \frac{1}{2} \sum_i m_i z_i^2 \tag{3.19}$$

At infinite dilution as $I \to 0$, the Debye and Hückel limiting law is obtained.

$$\ln \gamma_\pm = -3A_\phi |z_+ z_-| \sqrt{I} \tag{3.20}$$

This equation is an exact theoretical equation for dilute electrolyte solutions up to the ionic strength 0.001mol kg^{-1}. Many other modifications of the Debye and Hückel equation have been introduced later to improve the concentration range and the temperature dependency of the model.[37]

3.4 Pitzer ion interaction model

Pitzer proposed a model for non-dilute and mixed electrolyte solution.[38-41] The model is a virial expansion, which gives Gibbs excess energy in one kilogram of water and dissolved solutes species i, j,..., k with molalities m_i, m_j, …, m_k. The function $f(I)$, which is a modified Debye-Hückel term depends on the ionic strength I of the solution and the solvent properties.

$$\frac{G^E}{RTn_w M_w} = f(I) + \sum_i \sum_j \lambda_{ij}(I) m_i m_j + \sum_i \sum_j \sum_k \tau_{ijk} m_i m_j m_k + \ldots \tag{3.21}$$

$$f(I) = -A_\phi \frac{4I}{b} \ln(1 + b\sqrt{I}) \tag{3.22}$$

The empirical constant $b = 1.2$ kg$^{1/2}$ mol$^{-1/2}$ is used for all electrolytes. A_ϕ is given in (3.17) and I in (3.19). Interaction parameters $\lambda_{ij}(I)$ and τ_{ijk} are second and third virial coefficients and they represent the short- range interaction of two and three ions, respectively. If neutral components are present these parameters can be used for ion-neutral and neutral-neutral interactions. The model is constructed by means of measurable combinations of the parameters $\lambda_{ij}(I)$ and τ_{ijk}. For a single dissociating electrolyte MX ($M_{\nu_+}X_{\nu_-} = \nu_+ M^{z+} + \nu_- X^{z-}$, where exist ν_+ cations M and ν_- anions X with ionic charges z_+ and z_-) the mean activity $\gamma_\pm$ of a salt in the Pitzer formalism is given

$$\ln \gamma_\pm = -\left|z_+ z_-\right| A_\phi \left(\frac{I^{\frac{1}{2}}}{1+bI^{\frac{1}{2}}} + \frac{2}{b}\ln(1+bI^{\frac{1}{2}}) \right) + m_{MX} \frac{2v_+ v_-}{v}\left(2\beta_{MX}^{(0)} \right.$$

$$\left. + \frac{2\beta_{MX}^{(1)}}{a^2 I}\left[1 - \left(1 + \alpha\, I^{\frac{1}{2}} - \frac{\alpha^2 I}{2}\right)\exp(-\alpha\, I^{\frac{1}{2}})\right]\right) \tag{3.23}$$

$$+ \frac{3m_{MX}^2}{2}\left(\frac{2(v_+ v_-)^{\frac{3}{2}}}{v} C_{MX}^\phi \right) + \frac{2}{v} m_n \Lambda_{n,MX}$$

The values for constants in the equation are the same as presented earlier i.e. $\alpha = 2\,(\mathrm{kg}/\mathrm{mol})^{1/2}$, $b = 1.2\,(\mathrm{kg}/\mathrm{mol})^{1/2}$, A_ϕ is the temperature-dependent Debye-Hückel parameter and $v = v_+ + v_-$ is the sum of dissociated ions. Index n refers to dissolved gas and MX to salt, respectively. The parameters $\beta_{MX}^{(0)}$, $\beta_{MX}^{(1)}$, C_{MX}^ϕ are tabulated binary ion-ion interaction parameters. These Pitzer parameters are temperature-dependent and to a lesser degree pressure dependent. The neutral-ion interaction for dissolved salt MX with dissolved gas n is given by $\Lambda_{n,MX}$ in the Pitzer formalism. This can further be related to Setschenow's salting out/in coefficient $K_{n,MX}$.

$$K_{n,MX} = 2\Lambda_{n,MX}\,/\,2.303 \tag{3.24}$$
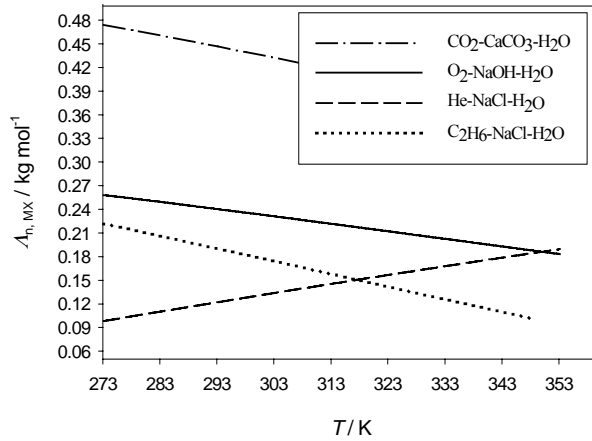
Figure 3-5. Temperature dependence of Pitzers binary ion-neutral interaction coefficient for dissolved salt $\Lambda_{n,MX}$. Estimation method was used to predict the salting out coefficient $K_{n,MX}$ that is related to $\Lambda_{n,\,MX}$.

Setschenow's constants usually decrease with increasing temperature and they are gas-specific. The temperature dependency of the constant is linear in a small temperature range. For mixed salts, the salting out coefficient is the sum of each ion's contribution in the mixture.[42,43] For oxygen dissolved in alkaline solution one obtains the following temperature dependent function for Pitzer ion-neutral parameter $\Lambda_{O_2,NaOH}$. The function is valid within 273- 353 K and 0- 1.2 mol kg^{-1} NaOH molalities.[43]

$$\Lambda_{O_2-\text{NaOH}} = 0.516 - 9.415 \cdot 10^{-4} \, T / K \tag{3.25}$$

Using Pitzer's treatment and the Gibbs-Duhem relation, a formula for the osmotic coefficient of water in electrolyte solution is obtained

$$\begin{aligned}
\phi - 1 = &- \left| z_M \, z_X \right| \frac{A_\phi I^{0.5}}{(1 + b I^{0.5})} + 2 m_{MX} \frac{\nu_M \nu_X}{\nu} \left[\beta_{MX}^{(0)} + \beta_{MX}^{(1)} \exp(-\alpha I^{0.5}) \right] \\
&+ m_{MX}^2 \frac{2(\nu_M \nu_X)^{3/2}}{\nu} C_{MX}^\phi
\end{aligned} \tag{3.26}$$

where ϕ is the osmotic coefficient of water in electrolyte solution, z_+ and z_- are the charges of positive and negative ions. In Figure 3-6, the mean activity coefficient and osmotic coefficient of sulphuric acid in water are shown at 25°C. In Figure 3-7, the dissociation of sulphuric acid into sulphate and bisulphate ions in water is shown at 25°C. In the calculations four binary Pitzer parameters obtained from literature were used.[35]
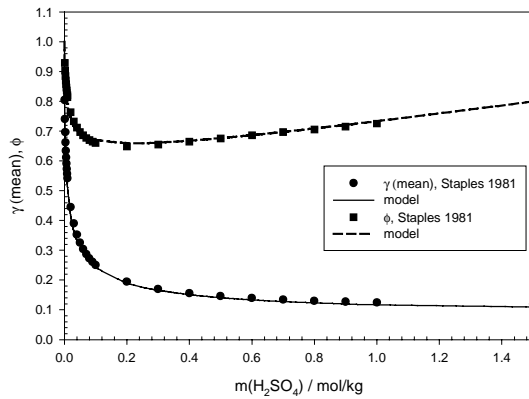

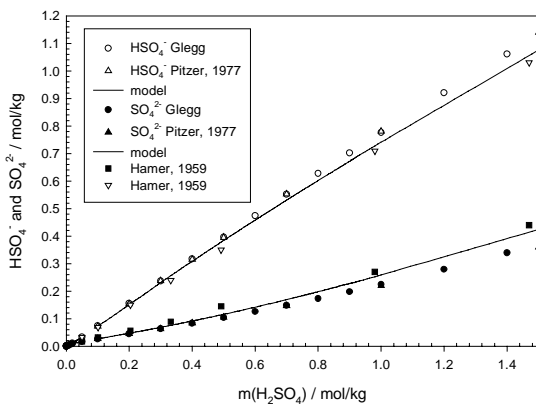**Figure 3-6.** The mean activity coefficient and osmotic coefficient of sulphuric acid in water at 25°C.[35,45]

Figure 3-7. The dissociation of sulphuric acid into sulphate and bisulphate ions in water at 25°C.[35, 46-48]

3.5 Other models for electrolyte solutions

Other models than Pitzer's have to be used in order to describe equilibrium in mixed aqueous solutions with electrolytes and dissolved gases. These include the development of electrolyte NRTL and Wilson, extended UNIQUAC and the modifications of UNIFAC models. Several additional difficulties arise in describing the electrostatic interaction in mixed solvents. A volatile organic component in water changes the structure of the solvent. The addition of salt increases the complexity of describing the short-range interactions, which are usually known for pure water-salt solutions at moderate temperatures. Also the long-range electrostatic interactions for ions are function of relative permittivity ε_r. The concentration dependence of relative permittivity has to be measured or estimated for mixed solvents if the Debye-Hückel equation is used in modified models. The development of mixed solvent models, is still dependent on the measured data. Recent publications include thermodynamic properties, VLE and salt effect data on salt-organic component- water systems.[49-52] The extended UNIQUAC model for the calculation of gas solubilities and salt solution was introduced by Sander (1984).[53] The model was constructed by adding the Debye-Hückel term into the original UNIQUAC equation by Prausnitz and Abrams (1975).[54] The model has been proven to calculate VLSE for some electrolyte solutions. Slightly modified models are described by several authors.[55-61]

4. PHYSICOCHEMICAL MODELLING OF BLEACHING SOLUTION AND REACTIONS

4.1 Background

The annual production of paper and paperboard is approximately 300 million tonnes worldwide. Paper products are made from natural fibres mostly, from wood material, which is processed with water, chemicals, minerals and heat. The principles of papermaking have been known for two thousand years and the process has grown into a highly technically integrated one. A pulp and paper mill is a huge complex that comprises many different stages, which include the grinding of the raw wood into small particles, pulping, (pulping = fibrous raw material is processed mechanically or chemically to fibrous mass), bleaching, washing, evaporation of water, drying and final processing in the paper machine. The typical production rate of dry cellulose pulp in a paper mill is around 400 000- 600 000 tons in a year. The amount of raw wood needed is several times more, and is equivalent to the loads of 300- 500 lorries arriving at the mill daily. The best available techniques and continuous improvements are needed to produce an environmentally acceptable, energy- efficient process, which requires an ever-smaller input of chemicals, fresh wood and water but an increased amount of re-circulated matter.[62-65]

4.2 Thermodynamic applications in the pulp and paper industry

The applications of thermodynamics cover a wide spectrum in the pulp and paper industry. Chemical thermodynamics provides a fundamental and widely applicable tool for studying multiphase solutions in the pulping and papermaking processes.[66] Modern processes recycle the water thus reducing the amount of fresh water needed in paper manufacturing. At the same time, the aqueous solutions become more concentrated with respect to the dissolved organic compounds and ions. Also the greenhouse gas CO_2 circulation plays a role in the overall environmental impact of any industrial process considered. Thermodynamics provides a practical tool for the estimation of the chemical states of pulp and paper solutions. Such a fundamental approach relates to the chemical energy, chemical reactions, solubility of gases and salts, and an important online process parameter pH.

4.3 Alkaline peroxide bleaching solution

Bleaching is the process of removing the lignin from wood by means of chemicals and heat, leaving a residue of cellulose material. Cellulose and hemicellulose are the main solid constituents of woody plants, which are chemically linear polysaccharides with a high molecular weight. As the lignin, the non-carbohydrate portion of the cell wall of the plant material is removed, the brightness of the pulp is increased. Common bleaching agents are chlorine dioxide, hypochlorite, hydrogen peroxide, oxygen, and ozone. The

choice of bleaching agent depends on the wood material itself, the chemical and energy costs, environmental issues and the quality of bleached fibres desired. Environmental concerns have forced the previously used hazardous chlorine gas, Cl_2 to be replaced with new chemicals, like peroxides. Hydrogen peroxide (H_2O_2), applied together with pressurized oxygen gas (O_2) has been studied as one alternative in total chlorine- free (TCF) bleaching. Oxygen-pressurized peroxide bleaching (PO) is carried out in this work at moderate oxygen pressures of 1- 20 bar (0.1- 2 MPa) and at elevated temperatures of 80- 120°C. The kinetics and thermodynamics of the process solution and the changes on the pulp properties are both needed for process optimization with respect to time, temperature, pressure, pulp consistency, and chemical charges. The Gibbs energy calculations together with measured solution and pulp properties give valuable information of the bleaching process. The reaction dynamics involve both the dissolved oxygen and the stabilized hydrogen peroxide as active species.

4.4 Gibbs energy model for H_2O_2-NaOH-O_2-H_2O system

The improved bleaching with the simultaneous use of hydrogen peroxide and oxygen in the alkaline environment is often considered to result from the increased perhydroxyl (OOH$^-$) ions that are formed due to hydrogen peroxide dissociation and its equilibration with NaOH. The alkaline solution dissociates hydrogen peroxide into proton and the reactive perhydroxide ion is expressed by the reaction equation H_2O_2(aq) $\Leftrightarrow$ H$^+$ + OOH$^-$ or similarly OH$^-$ + H_2O_2(aq) $\Leftrightarrow$ OOH$^-$ + H_2O, (aq = aqueous phase). The formation of different chemical species in the bleaching solution was assayed by using a multi-component thermodynamic model. With such a model, the equilibrium concentrations of various species at different temperatures and pressures can be surveyed by using a Gibbs energy minimization routine such as Chemsage and Chemsheet. With such a routine, the equilibrium composition of a chemical multicomponent system may be calculated at a given temperature and pressure. As the model calculates the Gibbs energy of the system in terms of the thermodynamic activities, pH also becomes calculated. At 298.15 K the calculation yields $K_P = 2.105 \cdot 10^{-12}$ for the equilibrium constant,

$$K_P = \frac{a_{H^+} a_{HO_2^-}}{a_{H_2O_2}}$$
(4.1)

The calculated K_P is in accordance with the NBS tables which gives a standard change of Gibbs energy $\Delta_r G^\circ$ =66647.8 J/mol for (4.1).[13] In addition, the numerical value K_P=2.4·10^{-12} ($\Delta_r G^\circ$ =66322.2 J/mol) has been reported at 25°C.[67] The model was constructed by selecting the gaseous and dissolved oxygen as a distinct image species. This is labelled as O_2* and it has the same thermodynamic properties as normal oxygen but it does not take part in the decomposition reaction of H_2O_2 in reaction

(4.4). By using this technique, separate equilibrium solubility can be calculated for oxygen, while the hydrogen peroxide is not allowed to decompose to oxygen and water in the multicomponent equilibrium system. The end result is a model for the metastable hydrogen peroxide-oxygen system in the alkaline solution. The image method of calculation is reasonable for the particular application, as the hydrogen peroxide actually remains in a dissociated form in pure (chelated) pulp- bleaching solution and its decomposition even at elevated temperatures in alkaline solution is relatively slow.[68-69] The calculation of pH in the solution requires a model for the ionic activity coefficients, which is obtained from the respective expression of the excess Gibbs energy by the Pitzer model, including interaction between the ionic and neutral solute species. The solubility of image oxygen O_2^* (4.5) and dissociation reaction (4.3) was calculated with the multicomponent thermodynamic model simultaneously preventing the decomposition reaction of hydrogen peroxide (4.4).

$NaOH \Leftrightarrow Na^+ + OH^-$ (allowed) (4.2)

$H_2O_2(a) \Leftrightarrow H^+ + OOH^-$ (allowed) (4.3)

$H_2O_2(a) \Leftrightarrow H_2O + 1/2O_2(g)\uparrow$ (constrained) (4.4)

$O_2^*(g) \Leftrightarrow O_2^*(aq)$ (allowed, image component) (4.5)

In order to study the alkaline peroxide bleaching solution, a multicomponent model was developed for the constituents that are shown in the previous reaction equations. The constituents used in the model are given in Table 4-1.

Table 4-1 The system components used for the H_2O_2-NaOH-O_2-H_2O system. q represents negative value of elementary charge of the species.

Phase	Component	System components			
		O	Na	H	q
Gas	H_2O	1	0	2	0
	H_2O_2	2	0	2	0
	O_2	2	0	0	0
Aqueous	H_2O_2	2	0	2	0
	O_2	2	0	0	0
	O_2^*	2	0	0	0
	Na^+	0	1	0	-1
	OH^-	1	0	1	+1
	OOH^-	2	0	1	+1
	H^+	0	0	1	-1
Solid	NaOH	1	1	1	0

For the Gibbs excess energy G^{ex}, Pitzer's virial model was used to derive the respective activity coefficients for solute species. The activity coefficients equations, used in the model in Pitzer formalism are presented as follows:

$$\ln \gamma_{Na^+} = f^{\gamma} + 2m_{OH}B_{Na-OH} + 2m_{OOH}B_{Na-OOH} + m_{Na}m_{OH}B'_{NaOH} + m_{Na-OOH}B'_{Na-OOH} \quad (4.6)$$

$$\ln \gamma_{OH^-} = f^{\gamma} + 2m_{Na}B_{Na-OH} + m_{Na}m_{OH}B'_{NaOH} \quad (4.7)$$

$$\ln \gamma_{OOH^-} = f^{\gamma} + 2m_{Na}B_{Na-OOH} + m_{Na}m_{OOH}B'_{Na-OOH} \quad (4.8)$$

$$\ln \gamma_{H^+} = f^{\gamma} + m_{Na}m_{OH}B'_{NaOH} + m_{Na-OOH}B'_{Na-OOH} \quad (4.9)$$

where

$$f^{\gamma} = -A_{\phi}\left(\frac{I^{\frac{1}{2}}}{1+bI^{\frac{1}{2}}} + \frac{2}{b}\ln(1+bI^{\frac{1}{2}})\right) \quad (4.10)$$

$$B_{ij} = \lambda_{ij}(I) = \beta_{ij}^0 + \beta_{ij}^1\left[\frac{2}{x^2}\left(1-(1+x)e^{-x}\right)\right] \quad (4.11)$$

$$B'_{ij} = \frac{d\lambda_{ij}}{dI} = -\beta_{ij}^1\frac{2}{Ix^2}\left(1-(1+x+\frac{x^2}{2})e^{-x}\right) \quad (4.12)$$

$$x = \alpha\sqrt{I} \quad (4.13)$$

$$I = \frac{1}{2}\sum_i m_i z_i^2 \quad (4.14)$$

The model could also be used to estimate the ionic concentrations as functions of temperature and pressure in alkaline peroxide solution. The Henderson model was used for approximation of the liquid-junction potential of the measured pH values described by Bates.[70] The pH measurements were performed using a tip- point electrode. The liquid-junction correction was made between the 3 mol dm^{-3} KCl solution and 0.0075, 0.017, 0.049, and 0.075 mol(NaOH)/kg(H$_2$O) solutions. The calculated theoretical pH yields values that are higher than measured if only the binary Pitzer ion interaction parameters for Na$^+$ and OH$^-$ are used. This could be explained by the interaction between the Na$^+$ and OOH$^-$ ions, which is expected to have a small effect on the pH of the solution. The liquid junction corrected pH- values were used to fit empirical parameters $\beta^{(0)}_{Na-OOH} = 0.040$ and $\beta^{(1)}_{Na-OOH} = -7.283$. The contribution of the parameter C^{ϕ}_{Na-OOH} is assumed to be zero in the dilute solution. The calculated and experimental liquid-junction corrected pH-values for NaOH-H$_2$O$_2$ solution are shown in Figure 4-1.
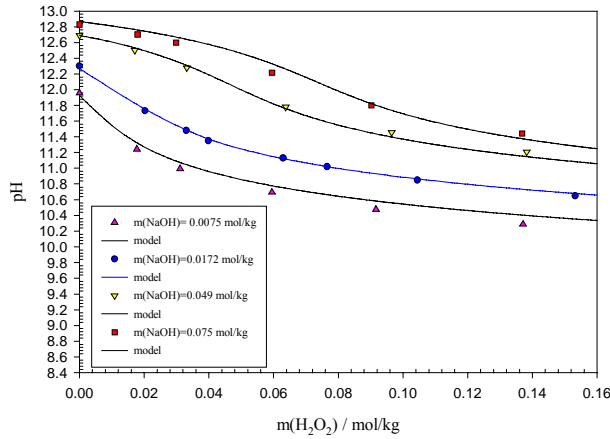
Figure 4-1. Experimental and calculated pH values are shown as a function of H_2O_2 molality in four different NaOH molalities at 24°C.

The calculations were further applied to simulate the chemical change in a heterogeneous system between a negatively charged fibre phase and an aqueous bulk phase. The potential difference $\varphi^\alpha - \varphi^\beta$ in the fibre α - water β solution is defined as the Donnan potential. While charges in the fibre are considered point charges, free ions in the water phase are divided unevenly in space, which satisfies the Poisson-Boltzmann distribution.[73] At constant temperature, the electrochemical equilibrium exists for those charged species that can cross the phase boundary. In macroscopic systems the electroneutrality condition (4.16) is assumed to be valid.

$$\mu_i^\alpha + z_i F \varphi^\alpha = \mu_i^\beta + z_i F \varphi^\beta \tag{4.15}$$

$$\sum_i z_i m_i = 0 \tag{4.16}$$

The Donnan potential leads to adsorption of counter ions into the fibre phase and noticeable pH change in the external solution. Consequently the addition of pulp fibres decreases the pH of the NaOH solution, especially close to neutral pH region.[74,75] The Donnan equilibrium constant D is further expressed by the ratio of the proton activities.

$$\Delta pH^\alpha = -\log a_{H^+}^\alpha = \text{pH(pure) - pH(pulp)} \tag{4.17}$$

$$D = \frac{a_{H^+}^\alpha}{a_{H^+}^\beta} = \frac{a_{Na^+}^\alpha}{a_{Na^+}^\beta} \tag{4.18}$$

where α, denotes the internal fibre and β, the external solution concentration, respectively. In Figure 4-2, the pH decrease is shown as a function of the fully bleached pulp consistency in four NaOH solutions. The adsorption of Na^+ ions lowers

the conductivity of the solution as the number of free charge carriers in the liquid phase decreases. The pH of the system decreases in a NaOH-water-pulp system as a function of added fibre consistency. An empirical equation $D = 0.756 \cdot I^{-0.711}$ was defined from pH dependence on pulp consistency at four different ionic strengths I of NaOH. The calculation can be further applied in such way that one can estimate the effect of the fibre on the pH and use it for estimating and controlling the pH in dilute alkaline systems close to the neutral region.
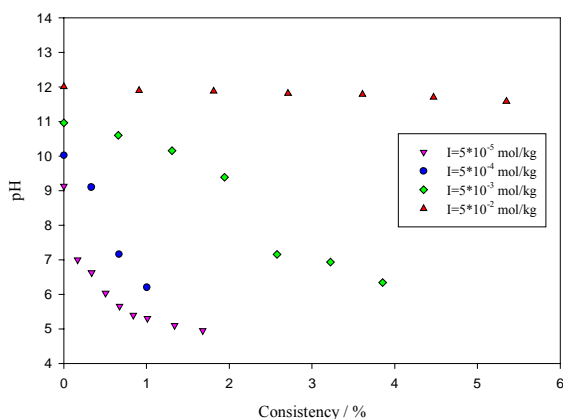

Figure 4-2. Measured pH values for bleached pulp as a function of pulp consistency at 25°C. The fibres were first washed with ion free water and with 0.1 M HCl solution in order to change the functional groups into hydrogen form. The concentration of bounded acidic groups (BAC) was defined as 35 mol/kg(fibre) by conductometric titration. The ionic strength I represents the initial ionic strength of the solution before the fibres have been added.

As the chemical amounts are changed in the model solution, the activity coefficient of the proton changes according to its functional composition dependence at constant T and P. For fully bleached (white) pulp, the pH change is assumed to be due to the neutralizing effect of bounded acid groups. In the brown pulp there are expected to be more carboxylic acid groups. In addition, also small amounts of precipitated acids and salts are dissolved in the solution.

4.5 Bleaching experiments

Experiments on reaction kinetics were performed with κ-12.9 and κ-9.6 pulp. The symbol κ represents the kappa number, a degree of delignification, where a decrease in the kappa number corresponds to the advancement in bleaching and increase in pulp brightness. The effects of temperature, pressure and chemical consumption on the pulp properties were measured as a function of time. In addition, the pH, peroxide and alkali consumption of the solution were determined as a function of the reaction time. The testing was performed in a Parr 4522 autoclave (2 000 cm^3), which had all internal components teflon-lined. Thus, the effect of surface oxidation and heterogeneous

catalysis on the vessel surface could be ignored when interpreting the experimental results.

Figure 4-3. Experimental set-up for (PO) bleaching studies. The pulp samples and the teflon mug are shown. The kappa numbers of the samples shown are from the left 7, 4, and 10.

The teflon mug on the lower right in Figure 4-3 is used to avoid contact between hydrogen peroxide and the steel surface of the pressurized reactor. Hydrogen peroxide is a highly reactive chemical, and in the presence of metal it will decompose into water and oxygen. In order to avoid the decomposition reaction of peroxide in the bleaching solution, the content of metal ions Mn^{2+}, Cu^{2+}, Fe^{3+}, Ca^{2+}, and Mg^{2+} that are naturally present are lowered by chelation, which mostly removes the undesired metal ions. EDTA (ethylenediaminetetraacetic acid) and DTPA (diethylenediaminepentaacetic acid) are commonly used to form chelates with transition metals before the peroxide bleaching takes place. The reaction kinetic experiments were performed with oxygen-bleached kraft pulp with initial κ-values 9.6 and 12.9. The pulp was pre-treated with DTPA to minimize the metal concentrations. The trace concentrations were analyzed with VG PlasmaQuad ICP-mass spectrometry, as shown in Table 4-2.

Table 4-2 The level of metals in parts per million (ppm) in the pulp samples. The analysis was carried out with VG PlasmaQuad ICP-mass spectrometry.

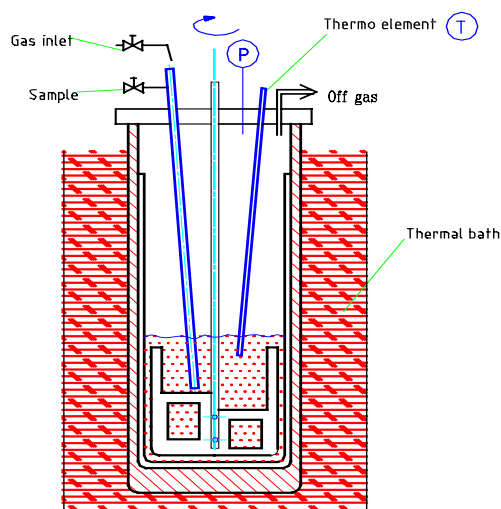| Pulp	Ca / ppm	Cu / ppm	Fe / ppm	Mg / ppm	Mn / ppm
κ-9.6	350	2.0	3	85	0.70
κ-12.9	<100	0.36	5	140	0.28

Figure 4-4. The experimental set up.

The experimental scheme was as follows. The desired amounts of sodium hydroxide and pulp were weighed and mixed. The alkaline pulp mixture was then thermostated and the weighed hydrogen peroxide-water solution was added by sampling using oxygen pressure. The pressure was set immediately at the desired partial pressure of oxygen. For each test, the final kappa-number, pulp brightness, pulp viscosity and residual alkali were analyzed. The pulp properties were determined with the following standard methods: kappa-number SCAN-C 1:77, viscosity SCAN-C 15:88 and ISO-brightness SCAN-C 11:75. The time-dependent data of pH and chemical consumption were recovered with a specially developed sampling technique. The pH of the recovered 5 ml samples were measured at circa 25°C by a tip-point electrode. The NaOH and H_2O_2 concentrations in the samples were defined by standardized HCl and iodometric titrations.

Table 4-3 Initial properties of the pulp and feed concentrations. The initial pH of the bleaching solution was set to 11.2 and consistency of the pulp was 5 %.

κ-number	Visco / dm^3/kg	Brightness / % ISO	NaOH-feed kg / t pulp	Peroxide-feed kg / t pulp
12.9	838	45.3	13.5	25
9.6	878	45.1	13.5	25

The experiments were performed at 80°C, 95°C, 110°C and 120°C, with oxygen partial pressures between 0.1 and 1.0 MPa. The bleaching reaction was found to be slow at 80°C temperature for κ- 9.6 and κ-12.9 pulp. In Table 4-4, the viscosity-, κ-reduction, brightness increase and residual alkali at 0.5 MPa and 95- 120°C bleaching tests are shown. Three experimental sets were performed for each temperature.

Table 4-4 Pulp properties from the PO-bleaching of κ-12.9 and κ-9.6 pulp at 5 % consistency at various temperatures and pressures. The alkali feed was 13.6 g / kg pulp and the peroxide feed was 25 g / kg pulp. All the experiments were of 120 minutes' duration.

κ-12.9	T / °C	$p(O_2)$/ MPa	Kappa- reduction %	Visco- reduction %	Brightness ISO Increase %	Residual alkali kg /t pulp
	95	0.15	43.4	3.5	43.1	6
	95	0.5	44.7	4.2	47.2	6.14
	95	1	48.1	5.1	50.2	5.5
	110	0.5	53.7	9.7	60.5	1.87
κ-9.6	96	0.5	37.5	11.3	69	5.57
	96	1.2	39.6	13.6	70.3	4.94
	110	0.5	45.8	19.4	73.4	1.25
	110	1.2	49	19.3	76.5	1.28
	120	0.5	43.8	14.6	61.9	0.58

In figure 4-5, the alkali consumption vs. the peroxide consumption in moles is outlined. It is interesting to note the change of the pattern of the alkali consumption at 120°C. The pulp properties and pH were also measured at timed intervals at ambient temperature. The measured changes of kappa- number and pH are plotted in Figure 4-6.
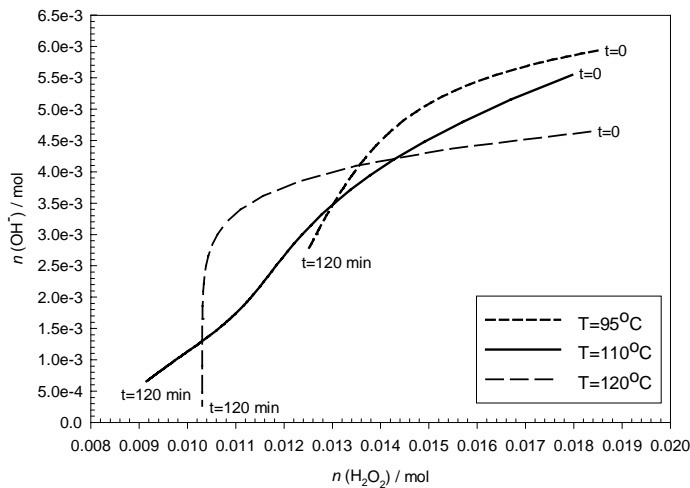

Figure 4-5. The observed alkali consumption vs. peroxide consumption in the PO-bleaching experiments where $p(O_2)$ = 0.5 MPa and κ (initial) = 9.6. The chemical consumption lines represent a 120-minute reaction from the beginning to the end of the reaction.
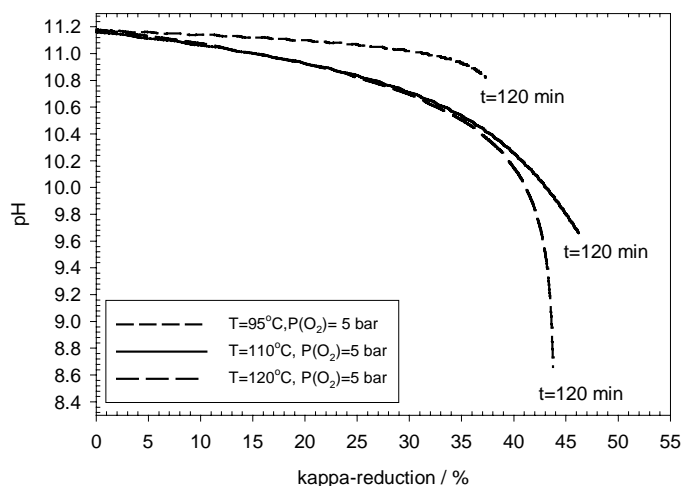
Figure 4-6. The decrease of pH as a function of kappa-reduction percentage. The endpoints of the curves represent a reaction of 120 minutes duration. The curves, which represent the reactions at 110 °C and 120 °C are identical to the point where the kappa-decrease is 31% and the corresponding pH is close to 10.7. The NaOH is increasingly consumed in non-desired neutralizing and surface reactions.

In Figure 4-7, the measured change of pH in the bleaching solution is shown as a function of the kappa- reduction percentage. The bleaching reaction was found to become more rapid as the temperature increased until a point was reached at each temperature where a further increase in bleaching time had an undesired effect on the final pulp quality. At a temperature of 120°C, the kappa- number reduces dramatically and stops completely after 25 minutes. The peroxide consumption was noticed to freeze but the alkaline continues to be consumed by other, neutralizing reactions. After this point, the alkaline is wasted and the quality of the fibre was found to decrease. The curves, which represent the reactions at 110°C and 120°C are identical to the point where the kappa-decrease is 31 % and the corresponding pH is 10.7. It takes 40 minutes for the 110°C reaction to reach this point and 25 minutes for the 120°C reaction. The effect of changing the temperature and pressure during the reaction was studied in order to simulate one stage and two- stage processes. It was evident from the measurements taken that raising the temperature from 110°C to 120°C during the reaction has a detrimental effect on the residual pulp properties.

4.6 Setting kinetic control for pH calculations

Within the framework of the applicability of the thermodynamics, one can relate the time-dependent changes to measurable quantities. The necessary but not sufficient requirement is that the standard state data and the activity coefficient model are valid within the temperature, pressure and composition range in equilibrium. Traditionally, the Gibbs energy change $\Delta_r G$ in chemical reaction is related to the extent of reaction ξ, i.e. related to the sum of chemical potentials of the reactants and products multiplied by the stoichiometric number. At equilibrium, the Gibbs energy is at the minimum, which

34

corresponds to a zero slope in the two-dimensional phase space, and the right-hand side of the equation (2.18) is zero. Systems that are strictly non-equilibrium processes can additionally be evaluated by the Gibbs energy approach on a point-by-point basis. The physical and chemical changes of the fluid properties should be measurable at each time-point. In the model calculations all the system state properties are defined in this dynamic chemical state that represents local equilibrium of the reactive solution. The question of how fast the reaction is cannot be answered by means of thermodynamics, and is a matter of chemical kinetics. During the chemical reaction the mole amounts of chemical constituents that are involved in the reaction are changed until equilibrium is reached. The time variable enters in to the thermodynamic calculation by using mass balance constraints in the model. The input mole amounts in these constraint equilibrium points are obtained using separately measured time-dependent composition of one or several components of the reactive solution or known kinetic path of the overall reaction. The thermodynamic multiphase model is then applied for calculation of the rest of the intensive properties like compositions including pH and extensive state properties. The knowledge of some system properties can be used for evaluating other properties in the studied system. This can be applied to various problems where one or some of the constituents of the reactive system are kinetically constrained.[4] The chemical as well as the energy changes are then calculated simultaneously as a function of the extent of the reaction or according to changing chemical amounts. This methodology has been applied in many fields of industrial processes with chemical reactions in the gas, liquid or solid phase. The addition of hydrogen peroxide into the alkaline solution containing 5 mass-% of fibres initiates the bleaching reaction. The heterogeneous reactions then consume alkaline and peroxide in solution, and the pH of the solution decreases. The reactions in the liquid phase were assumed to be fast. With this sequence, an empirical reaction rate expression for chemical consumption in the aqueous phase was combined with the Gibbs energy model by empirically determined mass balance conditions. A non-linear Levenberg-Marguardt algorithm was used to fit time-dependent functions for each set of experiments. The functions are given in Tables 4-5 and 4-6. The assumption in the dynamic multi-component model is that an equilibrium point is rapidly reached for reactions in the solution to obtain the minimum for the given chemical amounts and function $G(m_i, T, P)$. The changing chemical amounts of the reactants NaOH and H_2O_2 in the aqueous phase were given in the model as frozen equilibrium amounts. These chemical amounts represent the respective homogeneous equilibrium of the given chemical amounts. By using these composition data for H_2O_2 and NaOH, the pH as well as the rest of the system becomes calculated. At each given time point the pH is calculated and verified against measured values at ambient temperature. The measured and calculated pH sample values from 95°C and 110°C is shown in figure 4-7.

Table 4-5 The time-dependent functions for alkali consumption based on analyzed concentrations obtained from bleaching experiments. The alkali feed was 13.6 g(NaOH) / kg(dry pulp) in every experiment. The time t is in minutes.

$T / \,^\circ C$	g [NaOH] / kg pulp
95	$-0.039 \cdot t + 9.4937$
110	$-13.57 + 5.283 \exp(-0.0591 \cdot t) + 17.16 \exp(-0.00123 \cdot t)$
120	$0.3246 + 3.581 \exp(-0.0329 \cdot t) + 3.521 \exp(-0.0329 \cdot t)$

Table 4-6 The functions for peroxide consumption based on analyzed concentrations obtained from experiments. The peroxide feed was 1.15 g dm^{-3} in every experiment. The time t is in minutes.

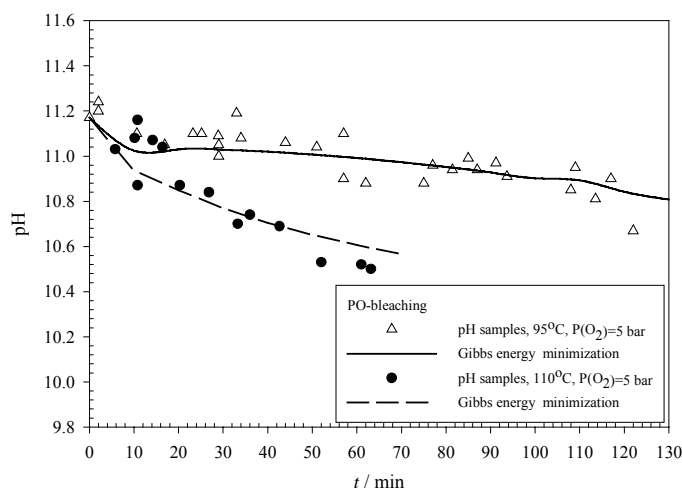| $T / \,^\circ C$	$[H_2O_2]$ / g dm^{-3}
95	$0.4492 + 0.2247 \exp(-0.04225 \cdot t) + 0.4905 \exp(-0.002878 \cdot t)$
110	$0.3237 + 0.3352 \exp(-0.1276 \cdot t) + 0.4724 \exp(-0.004818 \cdot t)$
120	$0.649 + 0.5061 \exp(-0.2318 \cdot t)$

Figure 4-7. Modelled and measured pH changes in the oxygen-pressurized peroxide bleaching reaction at 95°C and 110°C at 0.5 MPa oxygen partial pressure. The thermodynamic model could produce the pH of the reactive system up to 70 minutes of reaction time at 110°C and 120 minutes of 95°C.

Thermodynamic modelling and measurements were applied in the alkaline peroxide solution that is relevant for TCF bleaching. Both physico-chemical simulations and measurements of standard pulp properties are needed to understand the behaviour of the bleaching reaction. The use of kinetic control in the equilibrium calculations is useful for representation of the pH changes in the reactive systems. The calculated pH values were found to be in accordance with experimental values for reaction taking place at 95°C. At lower temperatures (80- 100°C), the reaction rates are relatively slow and the kappa-reduction is small. At each temperature, the decrease in kappa- numbers is more rapid in the beginning of the two-hour reaction but slows after approximately

10- 30 minutes. This can be noticed by a greater decrease of pH and alkaline consumption in the beginning. In calculations for aqueous solutions, a temperature-dependent standard data and activity coefficient model are needed to describe the total Gibbs energy for the solution. Process solutions involve complex reactions and electrochemical equilibrium between the fibre, ionic bulk solution, precipitates, and dissolved gases. As a result of the complex surface reactions on the fibres, alkaline and peroxide are consumed, organic acids formed, and a pH change is observed. The thermodynamic model gives useful information on the initial pH of the reactive bleaching solution at different alkaline and peroxide concentrations. The knowledge of the pH of the bleaching solution in the process is important as it influences the dissociation degree of hydrogen peroxide and the final pulp quality. The pH level should be kept around 11.3- 10.3 for the optimal results. Alkaline should not be added on the situation where it is extensively consumed in non-desired neutralization reactions. Both the knowledge of chemical changes and physical fibre properties are needed. The physical fibre properties, e.g. brightness, kappa- number, and fibre strength, are measured by standardized methods in laboratory studies. Obviously, the PO-stage combines the advantages of the alkaline oxygen bleaching and peroxide treatment. The reaction dynamics involves both the dissolved oxygen and the stabilized hydrogen peroxide as active species and thus the phenomena of PO-bleaching can be better understood through the thermochemistry of the alkaline hydrogen peroxide solutions. In many industrial processes, the pH is used as an online control parameter in combination with pressure and temperature. The knowledge of the pulp properties and the results of the model calculations can be used to reduce heating costs and the chemical charges in the bleaching process.

5. CARBON DIOXIDE EQUILIBRIUM AND REACTIONS IN AQUEOUS MEDIA

5.1 Multiphase CO_2-$CaCO_3$-H_2O system

With improving calculation routines and experimental knowledge, complex multiphase equilibrium and non-equilibrium systems can be successfully treated by a physicochemical approach.[6-8,76-84] Thermodynamics provides well-established scientific methodology for the evaluation of chemical reactions and equilibrium states related to carbon dioxide. The modelling of both the phase and chemical equilibrium provides a rigorous tool for studying aqueous industrial and environmental processes involving sources and sinks of CO_2.[85-93] Physicochemical methods together with laboratory experiments, pilot- and mill-scale experiences have also provided different applications in different fields of industries, where CO_2 is utilized as a reactant.[94-98] The relations of pH, chemical composition, partial pressure of CO_2 and precipitation and dissolution reactions of metal carbonate solids can be quantitatively treated by chemical thermodynamics.
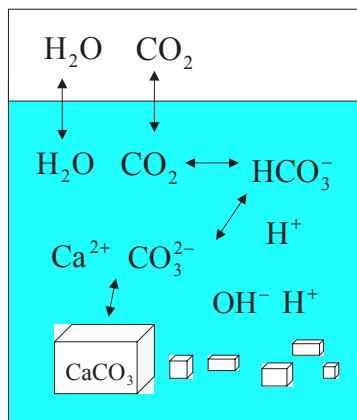

Figure 5-1. Carbon dioxide in aqueous calcite solution.

Generally, the identification of the appropriate reaction equations of a complex system is difficult. The calculation procedure based on the equilibrium constant in multicomponent solution includes iterative procedures, which are sensitive to the initial guess for the equilibrium molality. This can be avoided by using the minimization of the total Gibbs energy of the system. The equilibrium constant can be calculated backwards from the solution matrix, which gives the intensive properties like molalities and activities of the constituents involved in the chemical reactions. The results of the minimization routine can then be verified with literature data where equilibrium constants have been traditionally used. The reaction equations and the corresponding equilibrium constants for aqueous CO_2-$CaCO_3$ are given as follows:

$$CO_2(g) \Leftrightarrow CO_2(aq) \tag{5-1}$$

$$CO_2(aq) + H_2O \Leftrightarrow H^+ + HCO_3^- \tag{5-2}$$

$$HCO_3^- \Leftrightarrow H^+ + CO_3^{2-} \tag{5-3}$$

$$CaCO_3(s) \Leftrightarrow Ca^{2+} + CO_3^{2-} \tag{5-4}$$

The equilibrium constants of the previous reaction equations are given by means of total pressure P, molality m_i, activity a_i, fugacity coefficient ϕ_i, and activity coefficient γ_i of the individual species that take part on the chemical reactions.

$$K_H = \frac{a_{CO_2(aq)}}{f_{CO_2(g)}} = \frac{m_{CO_2(aq)} \gamma_{CO_2(aq)}}{y_{CO_2(g)} \phi_{CO_2(g)} P} \tag{5-5}$$

$$K_1 = \frac{a_{H^+} a_{HCO_3^-}}{a_{CO_2(aq)} a_{H_2O}} = \frac{m_{H^+} \gamma_{H^+} m_{HCO_3^-} \gamma_{HCO_3^-}}{m_{CO_2(aq)} \gamma_{CO_2(aq)} m_{H_2O} \gamma_{H_2O}} \tag{5-6}$$

$$K_2 = \frac{a_{H^+} a_{CO_3^{2-}}}{a_{HCO_3^-}} = \frac{m_{H^+} \gamma_{H^+} m_{CO_3^{2-}} \gamma_{CO_3^{2-}}}{m_{HCO_3^-} \gamma_{HCO_3^-}} \tag{5-7}$$

$$K_{sp} = a_{Ca^{2+}} a_{CO_3^{2-}} = m_{Ca^{2+}} \gamma_{Ca^{2+}} m_{CO_3^{2-}} \gamma_{CO_3^{2-}} \tag{5-8}$$

The calculated equilibrium constants are obtained from composition data at the minimum of the Gibbs energy justifying the validity of the input data of the model. Wagman NBS thermochemical data were used as input data in the Gibbs energy minimization routine in the calculations to produce the temperature dependent curves for the equilibrium constants K_H, K_1, and K_2, shown in figures 5-2, 5-3, and 5-4.[13] The solubility product K_{sp} is shown in the Figure 5-5.
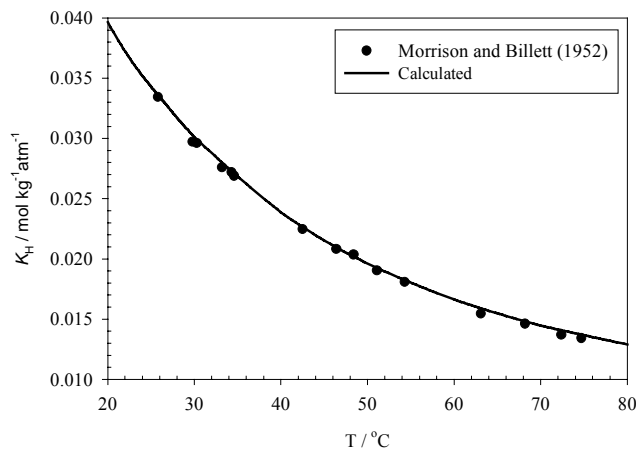

Figure 5-2. The equilibrium constant $K_H = a(CO_2,aq)/p(CO_2)$ for the reaction $CO_2(g) \Leftrightarrow CO_2(a)$ within 20- 80°C. The model values are compared with reference solubility data.[99]
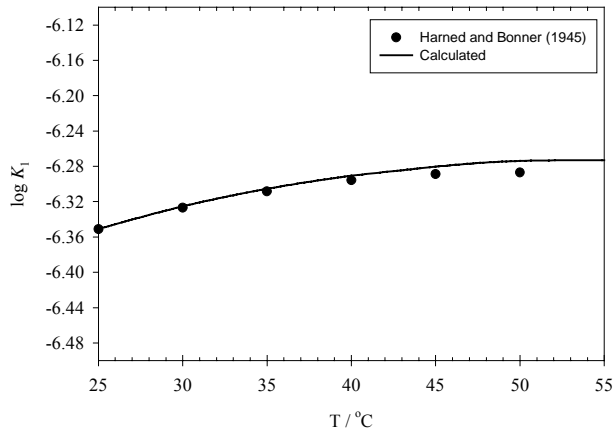
Figure 5-3. The equilibrium constant $\log K_1$ for the reaction $CO_2(aq)+H_2O \Leftrightarrow H^+ + HCO_3^-$ within 25-55°C. The calculated results are shown with reference data.[100]
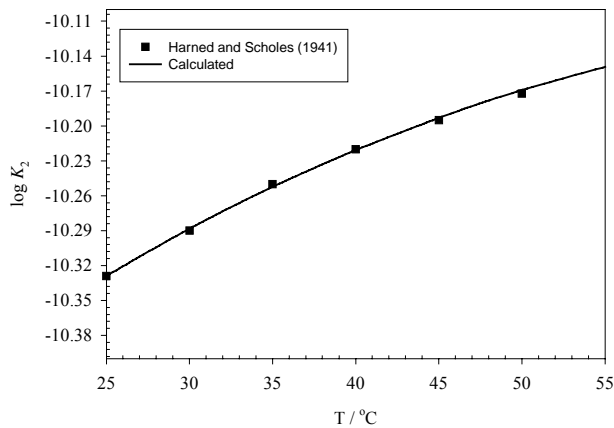

Figure 5-4. The equilibrium constant $\log K_2$ for the reaction $HCO_3^- \Leftrightarrow H^+ + CO_3^{2-}$ within 25-55°C. The model values are compared with reference data.[101]
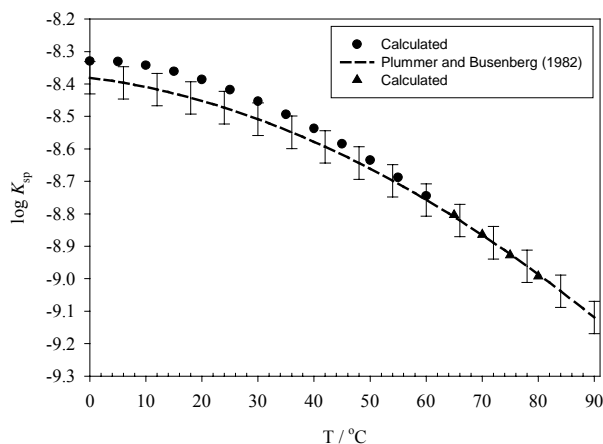

Figure 5-5. Solubility product of calcite $K_{sp} = a_{Ca^{2+}} a_{CO_3^{2-}}$ calculated using thermodynamic data by: ▲ Wagman (1982) NBS data[13] ● heat capacity data by Shock (1988).[102] The experimental function including error bars by Plummer and Busenberg (1982) is shown in the figure as a dotted line.[103]

The numerical values of the equilibrium compositions of the chemical reactions as well as pH=-log(a_H^+) values are determined through the multiphase thermodynamic model at the minimum of the Gibbs free energy at specified $p(CO_2)$ and T. In the Figure 5-6 the change of pH is shown as a function of added dissolved calcite in distilled water in equilibrium with 0.9687 bar partial pressure of carbon dioxide at 25°C.
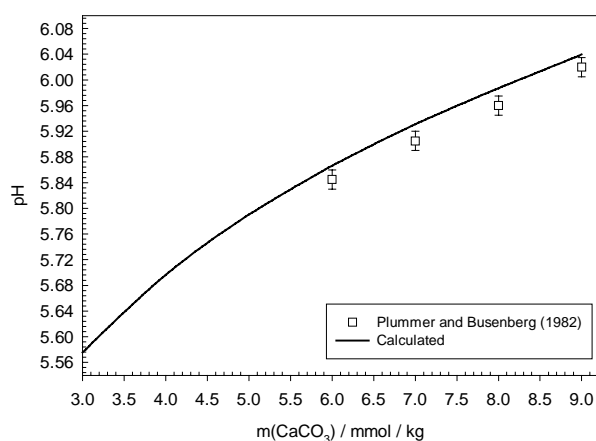

Figure 5-6. pH as a function of added dissolved calcite in distilled water at 0.9687 bar partial pressure of carbon dioxide at 25°C. The end point of the curve represents the saturated solution and the appearance of solid calcite phase. After this point the added calcite will stay in the solid phase and no change in the pH is observed.

The dissolution and precipitation processes of aqueous $CaCO_3$ solutions are controlled by the acid-base chemistry and it is a thermodynamically driven system. Thermodynamics gives quantitative knowledge of to what state the multiphase $CaCO_3$ solution will eventually reach if the temperature and pressure or chemical composition is altered. When calcium carbonate is present, the addition of the acid lowers the pH and increases the solubility. If sulphuric acid is also present, the overall reaction produces soluble calcium sulphate and carbon dioxide. The sulphuric acid H_2SO_4 dissociates in the water forming bisulphate HSO_4^- and sulphate SO_4^{2-} ions. When calcium carbonate is present the addition of the acid lowers the pH and increases the solubility of the carbonate, respectively. The addition of sulphuric acid raises the concentration of the protons H^+ and bisulphate HSO_4^- in the solution. The dissolution of calcium carbonate functions as a pH buffer through the formation of bicarbonate ions HCO_3^- as solid calcium carbonate dissolves. This gives the rise to $CO_2(aq)$ through (5.2) and (5.6). The effect of sulphuric acid on the pH in saturated $CaCO_3$ solution and non-buffered system under atmospheric CO_2 partial pressure is shown in the Figure 5-7.
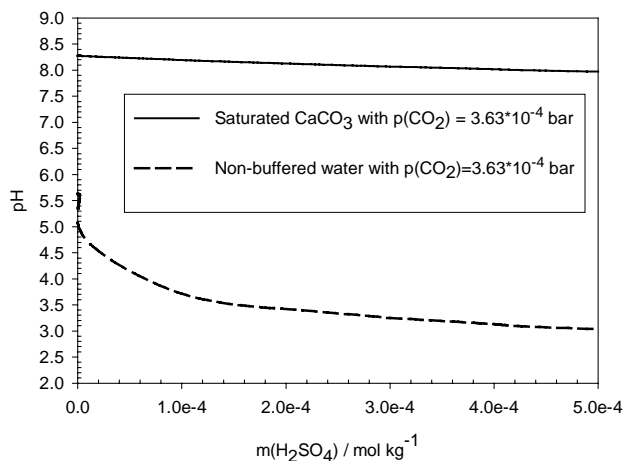
Figure 5-7. pH decrease in saturated $CaCO_3$ solution and non-buffered CO_2-water system at 25^oC in the addition of H_2SO_4. In saturated calcite solution circa 0.2 decrease of pH in the solution is reached by $2.55 \cdot 10^{-4}$ mol kg^{-1} sulphuric acid solution or doubling the CO_2 partial pressure from $3.63 \cdot 10^{-4}$ bar.

5.2 Solubility dynamics of calcite in the presence of carbon dioxide

The addition of sulphuric acid or carbon dioxide lowers the pH of the solution and initiates the dissolution of the solid particles with anionic ligands such as CO_3^{2-}, HCO_3^-, OH⁻. The protolysis equilibria of the anionic ligands at given $p(CO_2)$ fixes the pH at constant temperature. The reactions in solution will change the pH until equilibrium is reached at $p(CO_2)$ and T. The rate of equilibration can vary over orders of magnitude as the rates of dissolution reactions. The change of pH also reflects to the extent of the reaction and affinity and by measuring the pH one can follow the equilibration process of heterogeneous ionic system online. The increased molality of HCO_3^- raises the pH. In the solution mixture of divalent metal ions M^{2+} carbonates or hydroxide carbonates are precipitated.[88,104] In the following experiment, the dissolution reaction of calcite ($CaCO_3$) in CO_2 acidified water was studied by means of a multiphase Gibbs energy model. The pH curves are presented for the reactive system, as well as in equilibrium, as a function of dissolved calcite at 25 and 50^oC at a total pressure of 101.3 kPa. The partial pressures of CO_2 were calculated by reducing water vapour pressure from the total pressure, assuming Dalton's law to be valid.
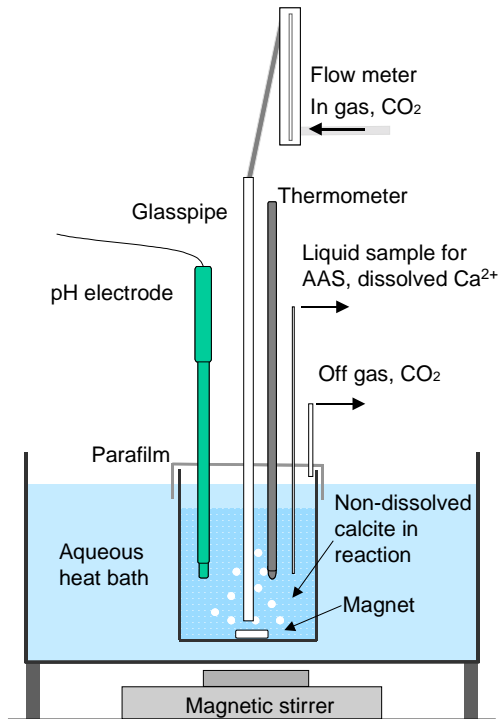
Figure 5-8. The experimental set up for pH measurements in the calcite dissolution process.[105] The Ca^{2+} samples for AAS analyzis were taken from the aqueous solution through 0.45 μm Millex-GS filters.

The experimental set up was as follows: 150.0 g of distilled water was poured in to a glass vessel, which was then covered and put in the heat bath with constant mixing using a magnetic stirrer. The temperature in the heat bath was set within $0.1^{o}C$ accuracy. The distilled water was then acidified by carbon dioxide under constant by-gas flow. After reaching solubility equilibrium of carbon dioxide, 100 mg of solid $CaCO_3$ (Baker, purity >99.0%) was weighed and added to the water solution. Typical particle size distribution of calcite in distilled water used in the experiments is shown in figure 5-9. The particle size has influence on the reaction kinetics as well as solubility of calcite.
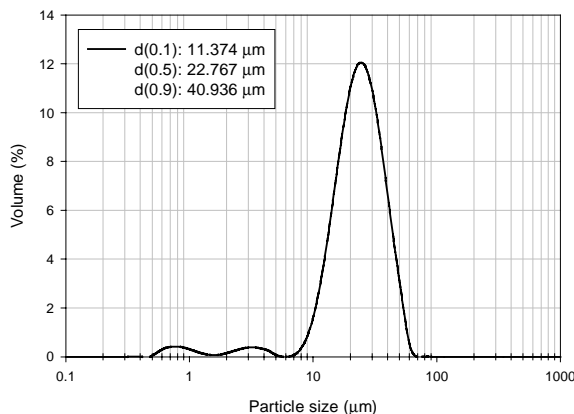

Figure 5-9. The size distribution of calcite particles in distilled water used in the experiments. The particle size analyzis were carried out with Malvern Mastersizer 2000.

43

The pH was measured on-line by a Metrohm 713 pH meter using a combined pH glass electrode (model 6.0238.00). The electrodes were calibrated with standard buffer solutions prior to each experiment at the temperature of the experiment. In Figure 5-10, typical pH curves are shown for the $CaCO_3$-CO_2-H_2O system with two different initial starting pH levels. In figure 5-11, two pH curves of freshly prepared calcite – distilled water solution and a solution exposed to air for two days are acidified with CO_2 at total pressure 101.3 kPa ($CO_2 + H_2O$) at 50^oC.

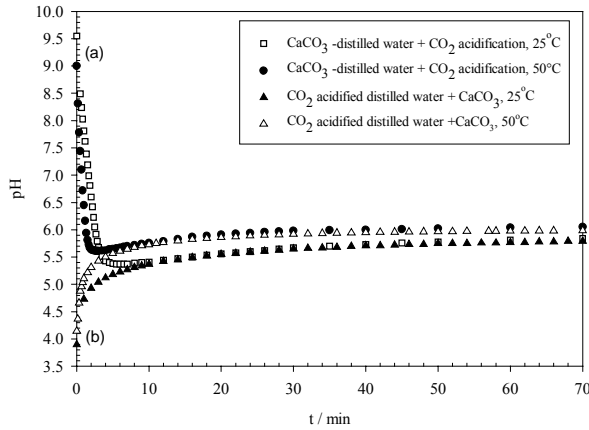**Figure 5-10.** The observed pH changes in $CaCO_3$-CO_2-H_2O system in two different starting points at basic- and acidic pH sides. (a) Freshly prepared calcite -distilled water solution result a basic solution that is acidified with CO_2 at total pressure 101.3 kPa ($CO_2 + H_2O$). (b) Distilled water acidified by CO_2 at total pressure 101.3 kPa ($CO_2 + H_2O$) results an acidic solution where calcite was added. The experiments were carried out at 25^oC and 50^oC. The observed pH change decreases as the solution approaches equilibrium at constant $p(CO_2)$ and T.
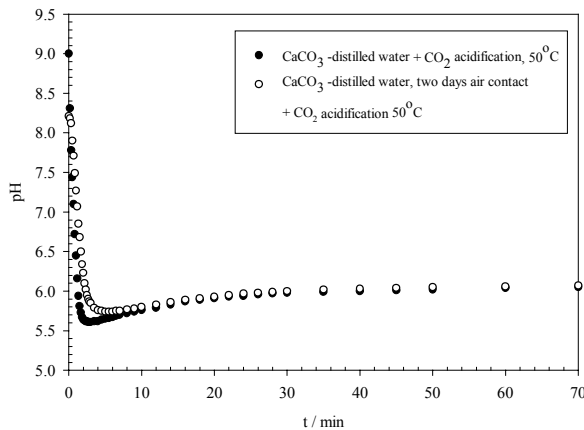
Figures 5-11. CO_2 acidification of two calcite solutions at total pressure 101.3 kPa ($CO_2 + H_2O$) at 50^oC. (a) Freshly prepared calcite –distilled water solution. (b) Solution exposed to air for two days. The initial pH is lower in the solution that was exposed into air due to dissolution of atmospheric carbon dioxide, $p(CO_2)$ =$3.63\cdot10^{-4}$ bar.

The Ca^{2+} content was analyzed from samples taken at different time points by Atomic Adsorption Spectrometry. The accuracy of the Ca^{2+} analysis was estimated to be $\pm(1-2)\%$. These analyzed chemical amounts of Ca^{2+} were used in the Gibbs energy minimization routine as feed amounts of dissolved calcium carbonate. An extended Debye-Hückel activity coefficient term from the Pitzer model was applied to describe the non-ideality of the ionic species in the Figures 5-12 and 5-13. The calculation yielded the corresponding homogeneous equilibrium in the aqueous phase with the given mass-balance constrains of Ca^{2+} satisfying the electroneutrality condition at given $p(CO_2)$ and T. The calculated pH values were then compared with online pH measurements at the same time point as the dissociation reaction of calcium carbonate advanced towards saturated solution.
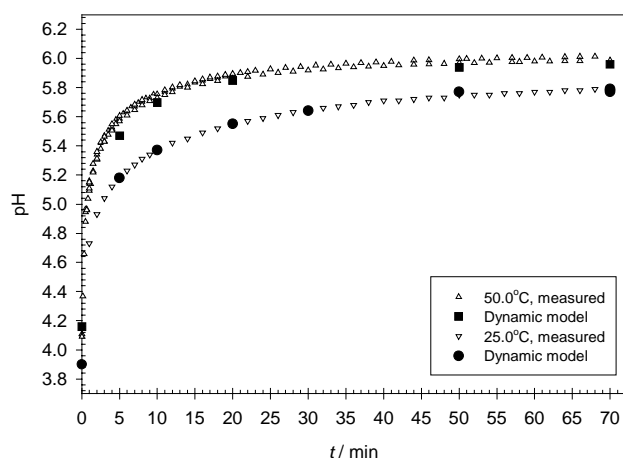
Figure 5-12. Calculated and measured pH values as a function of time at 25°C and 50°C in 101.3 kPa total pressure(CO_2 + H_2O). Independent AAS analyzed Ca^{2+} data were used in the model for pH calculations.
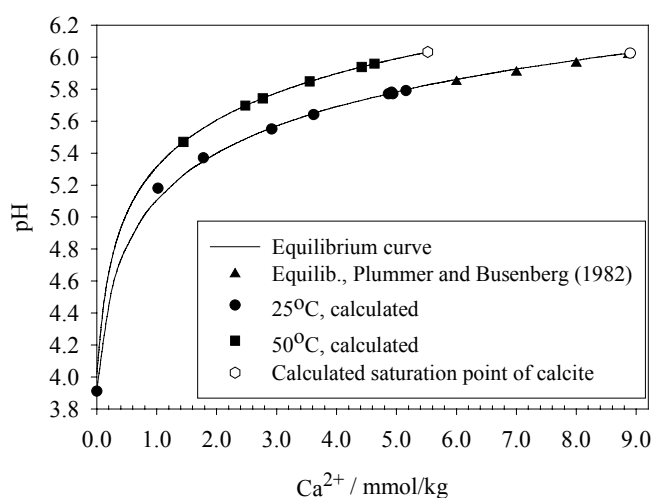

Figure 5-13. Calculated and measured pH values as a function of Ca^{2+} amount at 25°C and 50°C in 101.3 kPa total pressure. The results of the dynamic measurements and equilibrium values by Plummer and Busenberg[103] are also shown.

The equilibrium calculations can provide information on the system if the chemical changes are relatively slow. The time constant of the pH tip-point electrode is small compared to the reaction rate, and the samples taken are assumed to represent the state of the system at the time point considered. The $CaCO_3$ dissolution shown in Figure 5-12 strictly concerns non-equilibrium processes that can be calculated by the Gibbs energy approach using material balance restrictions for Ca^{2+} species. Each time point is related to the model calculation by the boundary conditions that are specific to the problem. At each time point, all the system state properties are defined for each step of given feed amounts. In Figures 5-14 and 5-15, the resulting Gibbs energy change and calculated entropy production are shown. For a closed system at constant temperature and pressure, the entropy production is expressed as the time derivative of the Gibbs energy function.[4] In this case, the entropy change $d_I S$ is due to the chemical changes of the closed system. The Gibbs energy should be a decreasing function and the entropy production positive for natural changes. In this system it is assumed to result from the chemical reaction that can be expressed through chemical potentials.

$$d_I S = -\frac{1}{T}\sum_i \mu_i d_i n_i \tag{2-15}$$

$$\frac{d_I S}{dt} = -\frac{1}{T}\frac{dG}{dt} \tag{5-9}$$
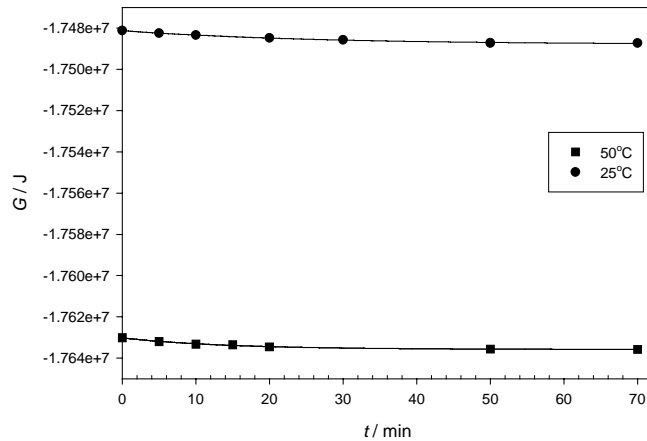
Figure 5-14. The decrease of the Gibbs energy of the system in the calcite dissolution process at 25°C and 50°C. The points represent the analysed Ca^{2+} chemical amounts shown in figure 5-13, and the respective calculated constrained equilibrium point of the reaction. The G is a contribution of all species over all phases and it is proportional to the volume of the system. As the dissolution process of $CaCO_3$ proceeds, the G is shown to decrease towards the global minimum of the reactive system.
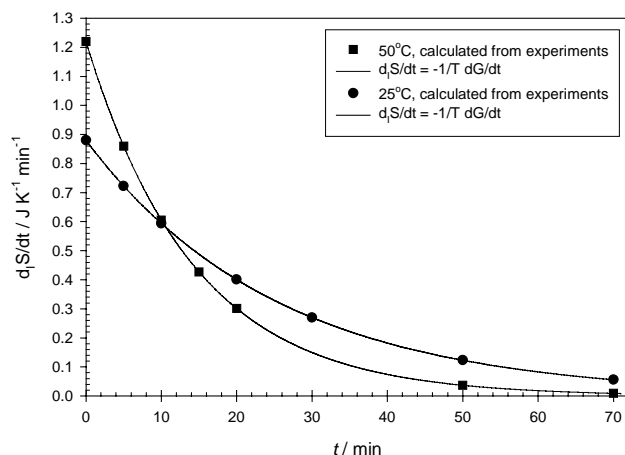
Figure 5-15. The entropy production during the dissolution process at 25°C and 50°C.

The calculations are thermodynamically consistent as the *G* value decreases during the dissolution reaction and the entropy production at constant temperature remains positive and approaches zero as the reaction proceeds towards equilibrium. The curves in Figure 5-15 show that at 50°C the dissolution process is faster than at 25°C, which is in accordance with the fact that the solubility of $CaCO_3$ is lower at 50°C than at 25°C, and at 70 minutes the equilibrium is closer for the reaction that occurs at 50°C.

5.3 The use of multiphase calcite chemistry in papermaking processes

The acid-base chemistry plays an important role in the papermaking process. The ways of controlling the process pH and maintaining it in a reasonable constant level have a major effect on the paper production rates. Calcium carbonate is used as a filler in making fine paper grades, like office paper. Carbon dioxide gas can be used as an alternative reactive acidifying chemical at the wet end of a paper machine in calcite buffered solutions, typically including 1- 2 mass % of fibres. The ions tend to build up and the precipitation of unwanted salts can occur as the water is circulated to reduce the amount of wastewater. By altering the carbon dioxide pressure, one can alter the pH and control the calcium carbonate precipitation and dissolution. Other natural sources of CO_2 exist in conditions favourable for biological activity.[85] The irreversible decomposition process of organic matter may then influence the pH level. The multi-component models could further be applied to model the wet -end chemistry of the paper machine, which includes the solid precipitate phases, the aqueous solution, and the air gases, including carbon dioxide. As for papermaking, sulphuric acid remains the major acidic substance used for pH control, although the use of carbon dioxide has been introduced with success, see also paper IV. The use of carbon dioxide as an alternative agent for controlling the pH of stock solutions has gained interest within the present day industry. In chemical pulp mills, dissolved CO_2 has been successfully used in increasing the efficiency of pulp washing by acidifying the stock from pH 10 to 6. The solubility of carbon dioxide in water is 55 times the solubility of air at room

temperature due to its weak electrolyte character. Traditionally the use of dissolved gases in the papermaking process has been avoided due to foaming or de-aeration problems. The overall solubility of CO_2 should not limit its use as a pH control if it is dissolved properly. Carbon dioxide will also bring H^+ ions to the system that inevitably dissolves $CaCO_3$, according to the overall reaction. However, when an excess of carbonate ions is led to the system, the common ion mechanism will influence in the opposite way such that the total effect results in a lower content of free calcium with CO_2 than with H_2SO_4 acidification. The solubility models are utilized in evaluating the conditions in the process circulation, where it is advantageous to dissolve inorganic material in the re-circulating parts and to enhance precipitation of calcium in the input. To decrease the solubility of $CaCO_3$, the common anion effect can be used, when carbon dioxide is chosen as the pH agent.[88]

6. CONCLUSIONS

Chemical thermodynamics shows the natural boundaries of the physical and chemical interactions as contributors in different chemical environments and in solutions where the reactions take place. Together, experiment, theory, and simulation play complementary roles in the development of applied thermodynamic models. The advantages using the Gibbs energy approach are that the extensive state properties are well defined and tested and have firm scientific basis. Furthermore, it allows simultaneous evaluation of the multicomponent multiphase solution including chemical reaction. Thermodynamic modelling and measurements were applied in the alkaline peroxide solution that is relevant for TCF bleaching. Both physico-chemical simulations and measurements of standard pulp properties are needed for understanding the behaviour of bleaching reaction. The use of kinetic control in the equilibrium calculations is useful for representation of the pH-changes in the reactive systems. The kinetics and thermodynamics of the process solution and the changes on the kraft pulp properties are both needed for process optimisation with respect to time, temperature, pressure, pulp consistency, and chemical charges. In many industrial processes, the pH is used as an online control parameter in combination with pressure and temperature. The knowledge of the pulp properties and the results of the model calculations can be used to reduce heating costs and the chemical charges in the bleaching process. The equilibrium and non-equilibrium chemistry of aqueous CO_2-$CaCO_3$ systems are important since these appear both in environmental systems as well as in industrial processes. This reaction processes between the solid, solution, and gas phases each have an effect on the equilibrium. The dissolution equilibrium of calcite is dependent on the proton activity $a(H^+)$ that can be altered by partial pressure of carbon dioxide in the gas phase. The general Gibbs energy method can be extended for specific dynamic processes that are usually treated by means of chemical kinetics. Dynamic constraints such as material restrictions can be included in the model for specific systems, giving additional value for the calculations based on the state functions and classical thermodynamics. The modern computer-aided multicomponent and multiphase calculation methods are rigorous methods for studying industrial processes that concern aqueous solutions. The pulp, paper and metal processing industries are fine examples of the successful integration of new methods into practice.

REFERENCES

[1]K. Denbigh, *The Principles of Chemical Equilibrium*, 3rd edition, Cambridge University Press, 1971.

[2]M. L. McGlashan, *Chemical Thermodynamics*, Academic Press, London, 1979.

[3]R. J. Silbey and R. A. Alberty, *Physical Chemistry*, 3rd edition, John Wiley & Sons, 2001.

[4]D. Kondepudi and I. Prigogine, *Modern Thermodynamics – From Heat Engines to Dissipative Structures*, John Wiley & Sons, 1998.

[5]S. Walas, *Phase Equilibria in Chemical Engineering*, Butterworth-Heinemann, 1984, p.337, 487-491.

[6]G. Erikson and K. Hack, Chemsage - a computer program for the calculation of complex chemical equilibria, Met. Trans. B. **21B**, 1013 (1990).

[7]P. Koukkari, K. Penttilä, K. Hack, and S. Petersen, ChemSheet – an efficient worksheet tool for thermodynamic process simulation, *Microstructures, Mechanical properties and process-computer simulation and modelling*, Y. Brechet (editor), Euromat99, Vol 3, Wiley-VCH, Berline, 2000, p.323.

[8]A. Roine, *HSC Chemistry for Windows*, User's guide, Version 5.1, Outokumpu Research Oy, Pori, Finland, 2001.

[9]E. Wilhelm, R. Battino, and J. Wilcock, Low-pressure solubility of gases in liquid water, Chem. Rew. **77**, 219 (1977).

[10]R. Perry, *Perry's Chemical Engineers' Handbook*, 6th edition, McGraw Hill, 1984.

[11]J. Prausnitz, R. Lichtenthaler, and E. Azevedo, *Molecular Thermodynamics of Fluid-Phase Equilibria*, 3rd edition, Prentice-Hall, 1999.

[12] D. Himmelblau, Solubilities of inert gases in water 0°C to near the critical point of water, J. Chem. Eng. Data. **5**, 10 (1960).

[13]Wagman et al., *The NBS Tables of Chemical Thermodynamic Properties*, J. Phys. Chem. Ref. Data. **11** (1982).

[14] I. Barin, *Thermochemical Data of Pure Substances*, VCH, Weinheim, 1989.

[15]J. Salminen, *Solubilities of Gases in Water Solutions*, Master's thesis, Helsinki University of Technology, Finland, 1997.

[16]T. Morrison, and F. Billett, The measurement of gas solubilities, J. Chem. Soc., 2033 (1948).

[17]J. Kratochvil, J. Sobr, J. Matous, and J. Pick, Solubilities of carbon dioxide in heavy water at pressures up to 40 atm, Collection Czechoslov. Chem. Commun. **35**, 3761 (1970).

[18]Å. Broden and R. Simonson, Solubility of oxygen part 1. Solubility of oxygen in water at temperatures $\leq$ 150°C and pressures $\leq$ 5 MPa, Svensk Papperstidning. **17**, 541 (1978).

[19]H. Clever and C. Han, Thermodynamics of aqueous systems with industrial applications, S. Newman, S. (editor), ACS Symposium Series **133**, 513 (1980).

[20]E. Narita, Solubility of oxygen in aqueous electrolyte solutions, Hydromet. **10**, 21 (1983).

[21]R. Battino, *Oxygen and Ozone*, IUPAC Solubility Data Series, Vol 7, Pergamon Press, Oxford, 1981.

[22]H. Pray, C. Schweickert, and B. Minnich, Solubility of Hydrogen, Oxygen, Nitrogen and Helium in water at elevated temperatures, Ind.Eng.Chem. **44** No 5, 1146 (1952).

[23]T. Rettich, R. Battino, and E. Wilhelm, Solubility of gases in liquids. 22. High-precision determination of Henry's law constant of oxygen in liquid water from T =274 K to T = 328 K, J. Chem. Thermodynamics **32**, 1145 (2000).

[24]D. Troman's, Temperature and pressure dependent solubility of oxygen in water: a thermodynamic analysis, Hydrometallurgy 327 (1998).

[25]A. Harvey, Semiempirical correlation for Henry's law constants over large temperature ranges, AIChE J. **42** No 5, 1491 (1997).

[26]A. Setschenow, Über die Konstitution der Salzlösungen auf Grund ihres Verhaltens zu Kohlensäure, Z. Phys. Chem. **IV**, 117 (1889).

[27] H. Corti, J. Pablo, and J. Prausnitz, Phase equilibria for aqueous systems containing salts and carbon dioxide. Application of Pitzer's theory for electrolyte solutions, J. Phys. Chem. **94**, 7876-7880 (1990).

[28] H. Corti, M. Krenzer, and J. Pablo, and J. Prausnitz, Effect of a dissolved gas on the solubility of an electrolyte in aqueous solution, Ind. Eng. Chem. Res. **29**, 1043-1050 (1990).

[29]F. A. Long and W. F. McDevit, Activity coefficients of nonelectrolyte solutes in aqueous salt solutions, Chem. Rev. **51**, 119 (1952).

[30]D. Troman's, Oxygen modeling in ammoniacal leaching solutions: leaching of sulphide concentrates, Minerals Eng. **13** No 5, 487 (2000).

[31]T. Kaskiala, Determination of oxygen solubility in aqueous sulphuric acid media, Min. Eng. J. **15** No 11, 853-857 (2002).

[32]D. Tromans, Modeling oxygen solubility in water and electrolyte solutions, Ind. Eng. Chem. Res. **39**, 805 (2000).

[33]W. Hayduk, *Final Report Concerning the Solubility of Oxygen in Sulphuric Acid-Zinc Pressure Leaching Solutions*, University of Ottawa, Ontario, 1991.

[34]G. Geffcken, Beitträge zur kenntnis der löslichkeitsbeeinflussung, Z. Phys. Chem. **49**, 257 (1904).

[35]H. Sippola, *Solubility of Ferrous Sulphate in Sulphuric Acid – a Thermodynamic Model*, Licentiate's thesis, Helsinki University of Technology, Finland, 1992.

[36]P. Debye and E. Huckel, The theory of electrolytes. I. Lowering of freesing point and related phenomena, Physik. Z. **24** 185, 334 (1923). Ref. from, H. Harned and B. Owen, *The Physical Chemistry of Electrolyte Solutions*, 2nd edition, Reinhold Publishing Corp. 1950, p.18.

[37]E. A. Guggenheim, *Thermodynamics*, 6th edition, North-Holland Publishing Company, Oxford, 1977.

[38]K. S. Pitzer, Thermodynamics of electrolytes. 1. Theoretical basis and general equations, J. Phys. Chem. **77**, 268 (1973).

[39]K. S. Pitzer, *Activity Coefficients in Electrolyte Solutions*, CRC Press, Boka Raton, Florida, USA, 1979.

[40]K. Pitzer, Electrolytes. From dilute solutions to fused salts, Am. Chem. Soc. **102:9**, 2902-2906 (1980).

[41]K. S. Pitzer, *Thermodynamics*, 3rd edition, McGraw-Hill, 1995.

[42]F. Millero, F. Huang, and L. Laferiere, The solubility of oxygen in the major sea salts and their mixtures at 25°C, Geochim. Cosmochim. Acta **66** No 13, 2349 (2002).

[43]A. Schumpe and S. Weisenberger, Estimation of gas solubilities in salt solutions at temperatures from 273 K to 363 K, AIChE J. **42** No 1, 298 (1996).

[44]W. J. Hamer and Y. C. Wu, Osmotic Coefficients and Mean Activity Coefficients of Univalent Electrolytes in Water at 25°C, J. Phys. Chem. Ref. Data **1**, 1047 (1972).

[45]B. R. Staples, Activity and osmotic coefficients of aqueous sulfuric acid at 298.15 K, J. Phys. Ref. Data, **10** No 3, 779 (1981).

[46]S. Glegg, J. Rard, and K. Pitzer, Thermodynamic properties of 0- 6 mol kg^{-1} aqueous sulfuric acid from 273.15 to 328.15 K, J. Chem. Soc. Faraday Trans. **90**, 1875 (1994).

⁴⁷K. S. Pitzer, R. N. Roy, and L. F. Silvester, Thermodynamics of Electrolytes 7. Sulphuric Acid, J. Am. Chem. Soc. 99 (1977).

⁴⁸W. Hamer, *The Structure of Electrolytic Solutions*, Wiley, New York, 1959.

⁴⁹R. Sun, Molecular thermodynamics of salt effect in vapour-liquid equilibrium of ethanol-water systems, Fluid Phase Eq. **157**, 29-40 (1999).

⁵⁰W. Wu et al., Modification of the further equation and correlation of the vapour-liquid equilibrium for mixed solvent electrolyte systems, Fluid Phase Equilib. **154**, 301-310 (1999).

⁵¹W. Yan, Prediction of vapour-liquid equilibrium in mixed-solvent electrolyte systems using the group contribution concept, Fluid Phase Equilib. **162**, 97-113 (1999).

⁵²M. Brendel and S. Sandler, The effect of salt and temperature on the infinite dilution activity coefficients of volatile organic chemicals in water, Fluid Phase Equilib. **165** No 1, 87-97 (1999).

⁵³B. Sander, *Extended UNIFAC/UNIQUAC Models for Gas Solubility Calculations and Electrolyte Solutions*, Ph.D. Thesis, DTU, Lyngby, Denmark,1984.

⁵⁴D. S. Abrams and J. M. Prausnitz, Statistical thermodynamics of liquid mixtures: A new expression for the Gibbs energy of partly of completely miscible systems, AIChE J. **21** No 1, 116-128 (1975).

⁵⁵K. Thomsen and P. Rasmussen, Modelling of vapor-liquid-solid equilibrium in gas-aqueous electrolyte systems, Chem. Eng. Sci. **54**, 1787-1802 (1999).

⁵⁶O. Chiavone-Filho and P. Rasmussen, Modelling salt solubilities in mixed solvents, Brasilian J. Chem. Eng. **7** No 2, 117-131 (2000).

⁵⁷K. Thomsen, *Aqueous Electrolytes: Model Parameters and Process Simulation*, Ph.D. Thesis, DTU, Lyngby, Denmark, 1997.

⁵⁸H. Nicolaisen, *Phase Equilibria in Aqueous Electrolyte Solutions*, Ph.D. Thesis, DTU, Lyngby, Denmark, 1994.

⁵⁹O. Chiavone-Filho, *Phase Behaviour of Aqueous Glygol Ether Mixtures: (1) Vapour-Liquid Equilibria (2) Salt Solubility*, Ph.D. Thesis, DTU, Lyngby, Denmark, 1993.

⁶⁰M. Iliuta, K. Thomsen, and P. Rasmussen, Modelling of heavy metal salt solubility using the extended UNIQUAC model, AIChE J. **48** 11, 2664-2689 (2002).

⁶¹W. Barbosa, J. Salminen, and O. Chiavone-Filho, Modeling of osmotic coefficient for a series of aqueous salt systems using the UNIQUAC+Debye-Hückel equation, 16th IUPAC Conference on Chemical Thermodynamics, ICCT-2000, P6c-MON-13, Halifax, Canada, 6-12.8.2000.

⁶²G. A. Smook, *Handbook for Pulp & Paper Technologists*, 3rd edition, Angus Wilde Publications Inc., Vancouver, 2002.

⁶³Kirk-Othmer, *Encyclopedia of Chemical Technology*, Vol 18, 4th edition, Wiley, 1996, p.1-60.

⁶⁴J. Gullichsen and H. Paulapuro (editors), *Papermaking Science and Technology*, Volumes 1-19, TAPPI Press, ISBN 952-5216-00-4, 1999-2001.

⁶⁵C.V. Dence and D.W. Reeve, *Pulp Bleaching, Principles and Practice*, TAPPI Press, Atlanta, Georgia, 1996.

⁶⁶J. Salminen and O. Antson, Physico-chemical modelling and experiments involving reactive aqueous solution, *Bunsen Discussion Meeting Global Phase Diagrams*, August 2001, Walberberg, Germany, Shaker Verlag, Aachen 2001, ISBN 3-8265-9130-5.

⁶⁷I. Freier, *Aqueous Solutions, Data for Inorganic and Organic Compounds*, Vol 2, Walter de Gruyter, 1978.

[68]R. Frederick, R. Duke, and W. Haas, The homogenous base -catalysed decomposition of hydrogen peroxide, J. Phys. Chem. **65**, 304 (1961).

[69]D. Lachenal, The potential of H_2O_2 as delignifying and bleaching agent. Application to new bleaching sequences, PanPacific Conference, Tokio, 1992, P1-l5.

[70]R. Bates, *Determination of pH- Theory and Practice*, Wiley, 1973.

[71]J. Salminen and P. Koukkari, Calculation of solubility of oxygen and pH in aqueous H_2O_2-NaOH-O_2-system using Pitzer-Setschenow model, Oral presentation, 15th IUPAC Conference on Chemical Thermodynamics, Porto, Portugal, 26.7-1.8.1998, C2-15.

[72]P. Koukkari, K. Penttilä, and J. Salminen, Chemsheet - a versatile worksheet tool for thermodynamic process simulation, 15th IUPAC Conference on Chemical Thermodynamics, Porto, Portugal, 26.7-1.8.1998, P7-4.

[73]R. Haase, *Thermodynamics of Irreversible Processes*, Addison Wesley, Massachusetts, 1969.

[74]F. Helfferich, *Ion Exchange*, McGraw-Hill, New York, 1962.

[75]J. Been and C. Oloman, Electrical conductivity of pulp suspensions using the Donnan equilibrium theory, JPPS. **21**, 80 (1995).

[76]R. Haase, On the relation between kinetics and thermodynamics for any number and kind of chemical reactions, Zeitschrift für Physikalische Chemie, Bd. **132**, 1-7 (1982).

[77]E. Königsberger and G. Eriksson, Simulation of Industrial Processes Involving Concentrated Aqueous Solutions, J. Sol. Chem. **28**, 721 (1999).

[78]Y. Liu and S. Watanasiri, Successfully Simulate Electrolyte Systems, Chem. Eng. Prog. **10**, 25 (1999).

[79]J. B. Christian, Simulating Aqueous Processes, Chem. Eng. Prog. **9**, 32-39 (2003).

[80]G. Eriksson, K. Hack, and S. Petersen, ChemApp – A Programmable Thermodynamic Calculation Interface, Werkstoffswoche'96, Symposium 8, Simulation Modellierung, Informationsysteme, Frankfurt, Germany, 1997, p.47.

[81]K. Hack, *The SGTE Casebook, Thermodynamics at Work*, Materials Modeling Series, The Institute of Materials, Borne Press, Bournemouth, 1996.

[82]N. Saunders and A. Miodownik, *CALPHAD, Calculation of Phase Diagrams*. Pergamon, 1998.

[83]Letcher, T.M. (editor), *Chemical Thermodynamics, IUPAC – Chemistry for the 21st Century*, Blackwell Science, 1999.

[84]Y. Demirel, *Nonequilibrium Thermodynamics, Transport and Rate Processes in Physical and Biological Systems*, 1st edition, Elsevier, 2002.

[85]P. Kobylin, J. Salminen, A. Ojala, and S. Liukkonen, Multiphase thermodynamics for CO_2 in natural systems, Sixth Finnish Conference of Environmental Sciences, Joensuu, Finland, 8-9.5.2003, Proceedings, p.145-146.

[86]M. E. Q. Pilson, *Introduction to the Chemistry of the Sea*, Pearson Education POD, 1st edition, 1998.

[87]J. N. Butler, *Ionic Equilibrium. Solubility and pH Calculations*, John Wiley & Sons Inc., 1998.

[88]D. Langmuir, *Aqueous Environmental Geochemistry*, Prentice Hall, 1997.

[89]P. Scharlin, *Carbon Dioxide in Water and Aqueous electrolyte Solutions*, IUPAC Solubility data Series, Volume 62, Oxford University Press, 1996.

[90]G. T. Hefter and R. P. T. Tomkins (editors), *The Experimental Determination of Solubilities*, Wiley Series in Solution Chemistry, Volume 6, John Wiley & Sons Ltd., 2003.

[91]S. A. Newman (editor), *Thermodynamics of Aqueous Systems with Industrial Applications*, ASC symposium series 133, ACS, Washington, 1980.

[92]T. Edwards, G. Mauer, J. Newman, and J. Prausnitz, Vapor-liquid equilibria in multikomponent aqueous solutions of volatile weak elektrolytes, AIChE J. **24** No 6, 966-976 (1978).

[93]J. Salminen, P. Koukkari, R. Pajarre, and Liukkonen, Multicomponent calculations and database-development with aqueous process solutions. Proceedings of Equifase 99, Vigo, Spain, 20-24.6.1999, Libro de Actas, Tomo II, p. 433-437.

[94]J. Salminen, Thermochemical Multiphase Models for General Chemistry and Paper Industry, Particles 2003, Imaging, Printing and Marking Applications of Particle Technology, AIChE, Toronto, Canada, 23-26.8.2003, C1-Invited Oral Presentation.

[95]H. Pakarinen and H. Leino, Benefits of using carbon dioxide in the production of DIP containing newsprint, *9th PTS-CTP Deinking Symposium*, Munich, Germany, May 9-12, 2000.

[96]P. Komulainen, *Modeling of the Dynamic Chemical State of De-Inked Pulp*, Masters thesis, Helsinki University of Technology, Finland, 2000.

[97]J.-P. Ylen, Measuring, *Modelling and Controlling the pH Value and the Dynamic Chemical State*, Ph. D. Thesis, Helsinki University of Technology, Finland, 2001.

[98]E. J. Beckman, Green chemical processing using CO_2, Ind. Eng. Chem. Res. **42**, 1598-1602 (2003).

[99]T. Morrison and F. Billett, The salting out of non-electrolytes. Part II. The effect of variation in non-electrolyte, J. Chem. Soc. 3819 (1952).

[100]H. Harned and F. Bonner, The first ionization of carbonic acid in aqueous solutions of sodium chloride, J. Am. Chem. Soc. **67**, 1026 (1945).

[101]H. Harned and S. Scholes, The ionization constant of HCO_3^- from 0 to 50^oC, J. Am. Chem. Soc. **63**, 1706 (1941).

[102]E. L. Shock and H. C. Helgeson, Calculation of the thermodynamic and transport properties of aqueous species at high pressures and temperatures: Correlation algorithms for ionic species and equation of state predictions to 5 kbar and 1000 ºC, Geochimica et Cosmochimica Acta. **52,** 2009 (1988).

[103]L. Plummer and E. Busenberg, The solubilities of calcite, argonite and vaterite in CO_2-H_2O solution between 0 and 90^oC, and an evaluation of the aqueous model for the system $CaCO_3$-CO_2-H_2O, Geochimica et Cosmochimica Acta. **46**, 1011 (1982).

[104]H. Gamsjäger and E. Königsberger, Solubility of sparingly soluble ionic solids in liquids, in G. T. Hefter and R. P. T. Tomkins (editors), *The Experimental Determination of Solubilities*, Wiley Series in Solution Chemistry, Volume 6, John Wiley & Sons Ltd., 2003, p.315-358.

[105]J. Salminen, P. Kobylin, T. Nissinen, and Liukkonen S., Process modeling involving aqueous solutions, Thermodynamics 2001, *Thermodynamics and Statistical Mechanics with Industrial Applications*, Bristol, UK, 4-6.4.2001.

APPENDIX
A1. Pitzer ion-interaction model
The excess Gibbs energy in Pitzer formalism gives

$$\frac{G^E}{RTn_wM_w} = f(I) + \sum_i \sum_j \lambda_{ij}(I)m_im_j + \sum_i \sum_j \sum_k \tau_{ijk}m_im_jm_k + \ldots \tag{A.1}$$

The function $f(I)$, which is a modified Debye-Hückel term depends on the ionic strength I of the solution and the solvent properties.

$$f(I) = -A_\phi \frac{4I}{b}\ln(1 + b\sqrt{I}) \tag{A.2}$$

$$I = \frac{1}{2}\sum_i m_iz_i^2 \tag{A.3}$$

The empirical constant b =1.2 $kg^{1/2} mol^{-1/2}$ is used for all electrolytes. A_ϕ is the osmotic Debye- Hückel parameter. Interaction parameters $\lambda_{ij}(I)$ and τ_{ijk} are analogous to second and third virial coefficients and represents the short range interaction of two and three ions, respectively. If neutral components are present these parameters can be used for ion-neutral and neutral-neutral interactions. The model is constructed by means of measurable combinations of the parameters $\lambda_{ij}(I)$ and τ_{ijk}. For an electrolyte with cations c, c'… and anions a, a'…the following simplifying combinations of $\lambda_{ij}(I)$ and τ_{ijk} are defined:

$$B_{ca} = \lambda_{ca} + \frac{v_c}{2v_a}\lambda_{cc} + \frac{v_a}{2v_c}\lambda_{aa} \tag{A.4}$$

$$\Phi_{cc'} = \lambda_{cc'} - \frac{z_{c'}}{2z_c}\lambda_{cc} - \frac{z_c}{2z_{c'}}\lambda_{c'c'} \tag{A.5}$$

$$C_{ca} = \frac{3}{2}\left(\frac{\tau_{cca}}{z_c} + \frac{\tau_{caa}}{z_a}\right) \tag{A.6}$$

$$\Psi_{cc'a} = 6\tau_{cc'a} - \frac{3z_{c'}}{z_c}\tau_{cca} - \frac{3z_c}{z_{c'}}\tau_{c'c'a} \tag{A.7}$$

with corresponding expressions for $\Phi_{aa'}$ and $\Psi_{aa'c}$. The excess Gibbs energy then becomes

$$\frac{G^E}{RTn_w M_w} = f(I) + \sum_c \sum_a m_c m_a \left[B_{ca} + \left(\sum_c m_c z_c \right) C_{ca} \right]$$

$$+ \sum_{c<c'} \sum m_c m_{c'} \left(2\Phi_{cc'} + \sum_a m_a \Psi_{cc'a} \right) \qquad (A.8)$$

$$+ \sum_{a<a'} \sum m_a m_{a'} \left(2\Phi_{aa'} + \sum_c m_c \Psi_{caa'} \right) + 2\sum_n \sum_c m_n m_c \lambda_{nc}$$

$$+ 2\sum_n \sum_a m_n m_a \lambda_{na} + 2\sum_{n<n'} \sum m_n m_{n'} \lambda_{nn'} + \sum_n m_n^2 \lambda_{nn} + \dots$$

The double-summation sub indices, c<c',a<a' and n<n' denote the sums over all distinguishable pairs of different cations, anions and neutral solutes. The individual ion activity coefficients obtained by standard thermodynamic relation:

$$\ln \gamma_i = \frac{\partial\, G^E}{RTn_w M_w \partial\, n_i} = z_i^2 F + 2\sum_j \lambda_{ij} m_j + \sum_{jk} m_j m_k \left(\frac{z_i^2}{2} \frac{d\lambda_{ij}}{dI} + 3\tau_{ijk} \right) \qquad (A.9)$$

Activity coefficient equations in Pitzer scale are shown as follows. Sub-index n refers to the neutral and c and a to ionic species respectively.

$$\ln \gamma_{+,M} = z_+^2 F + \sum_a m_a \left(2B_{Ma} + ZC_{Ma} \right) + \sum_c m_c \left(2\Phi_{Mc} + \sum_a m_a \Psi_{Mca} \right) \qquad (A.10)$$

$$+ \sum_{a<} \sum_{a'} m_a m_{a'} \Psi_{Maa'} + z_+ \sum_c \sum_a m_c m_a C_{ca} + 2\sum_n m_n \lambda_{nM} + \dots$$

$$\ln \gamma_{-,X} = z_-^2 F + \sum_c m_c \left(2B_{Xc} + ZC_{Xc} \right) + \sum_a m_a \left(2\Phi_{Xa} + \sum_c m_c \Psi_{Xca} \right) \qquad (A.11)$$

$$+ \sum_{c<} \sum_{c'} m_c m_{c'} \Psi_{cc'X} + |z_-| \sum_c \sum_a m_c m_a C_{ca} + 2\sum_n m_n \lambda_{nX} + \dots$$

The mean activity coefficient of a single salt MX then yields

$$\ln \gamma_{\pm,MX} = |z_+ z_-| F + \frac{v_+}{v} \sum_a m_a \left(2B_{Ma} + ZC_{Ma} + 2\frac{v_-}{v_+} \Phi_{Xa} \right) + \qquad (A.12)$$

$$\frac{v_-}{v} \sum_c m_c \left(2B_{cX} + ZC_{cX} + 2\frac{v_+}{v_-} \Phi_{Mc} \right) + \sum_c \sum_a m_c m_a v^{-1} \left(2v_+ z_+ C_{ca} + v_+ \Psi_{Mca} + v_- \Psi_{caX} \right) +$$

$$\sum_{c<} \sum_{c'} m_c m_{c'} \frac{v_-}{v} \Psi_{cc'X} + \sum_{a<} \sum_{a'} m_a m_{a'} \frac{v_+}{v} \Psi_{Maa'} + \frac{2}{v} \sum_n m_n \left(v_+ \lambda_{nM} + v_- \lambda_{nX} \right)$$

where

$$F = -A_\phi \left(\frac{I^{\frac{1}{2}}}{1+bI^{\frac{1}{2}}} + \frac{2}{b}\ln(1+bI^{\frac{1}{2}}) \right) + \sum_c \sum_a m_c m_a B'_{ca}$$
$$+ \sum_{c<} \sum_{c'} m_c m_{c'} \Phi'_{cc'} + \sum_{a<} \sum_{a'} m_a m_{a'} \Phi'_{aa'} \tag{A.13}$$

also

$$Z = \sum_i m_i |z_i| \tag{A.14}$$

$$B^\phi_{ca} = B_{ca} + IB'_{ca} \tag{A.15}$$

$$\Phi^\phi_{cc'} = \Phi_{cc'} + I\Phi'_{cc'} \tag{A.16}$$

$$C_{MX} = \frac{C^\phi_{MX}}{2|z_+ z_-|^{1/2}} \tag{A.17}$$

$$C_{MX} = \frac{3}{2}(\tau_{cca} + \tau_{caa}) \tag{A.18}$$

B' and Φ' are ionic-strength derivatives of B and Φ. Empirical expressions for ionic strength that are defined in a functional form, which includes the binary ion-ion interaction parameters β^0_{MX}, β^1_{MX} and β^2_{MX}

$$B^\phi_{MX} = \beta^0_{MX} + \beta^1_{MX} \exp(-\alpha_1 I^{1/2}) + \beta^2_{MX} \exp(-\alpha_2 I^{1/2}) \tag{A.19}$$

$$B_{MX} = \beta^0_{MX} + \beta^1_{MX} g(\alpha_1 I^{1/2}) + \beta^2_{MX} g(\alpha_2 I^{1/2}) \tag{A.20}$$

$$B'_{MX} = \frac{\beta^1_{MX} g'(\alpha_1 I^{1/2}) + \beta^2_{MX} g'(\alpha_2 I^{1/2})}{I} \tag{A.21}$$

where functions g and g' are given by

$$g(x) = \left[\frac{2}{x^2}\left(1 - (1+x)e^{-x}\right) \right] \tag{A.22}$$

$$g'(x) = -\frac{2}{x^2}\left(1 - (1+x+\frac{x^2}{2})e^{-x}\right) \tag{A.23}$$

where
$$x = \alpha_i \sqrt{I} \tag{A.24}$$

Parameters $\beta^{(0)}_{MX}$, $\beta^{(1)}_{MX}$ and $\beta^{(2)}_{MX}$ are solute specific and are fitted to isothermal or isobaric data for single electrolyte solutions. $\beta^{(2)}_{MX}$ is used for 2-2 of higher-valence

electrolytes that show a tendency of towards electrostatic ion pairing. For solutions containing univalent ions $\alpha_1 = 2.0 \text{kg}^{1/2}\text{mol}^{-1/2}$ and $\alpha_2 = 0$.

For 2-2 electrolytes $\alpha_1 = 1.4 \text{kg}^{1/2}\text{mol}^{-1/2}$ and $\alpha_2 = 12 \text{kg}^{1/2}\text{mol}^{-1/2}$ at 25°C. α_1 is independent of temperature but theories suggest that α_2 is proportional to the Debye-Hückel parameter A_ϕ. The Φ terms have strong ionic-strength dependence for unsymmetrical salts due to the long-range electrostatic forces. The expressions for Φ_{ij} are

$$\Phi_{ij} = \theta_{ij} + {}^E\theta_{ij}(I) \tag{A.25}$$

$$\Phi_{ij}' = {}^E\theta_{ij}'(I) \tag{A.26}$$

$$\Phi_{ij}^\phi = \theta_{ij} + {}^E\theta_{ij}(I) + I^{E}\theta_{ij}'(I) \tag{A.27}$$

where ${}^E\theta_{ij}(I)$ and ${}^E\theta_{ij}'(I)$ account for electrostatic unsymmetrical mixing effects and depend only on charges of ions i and j, the total ionic strength, density and dielectric constant of the solvent, temperature and pressure. The term θ_{ij} is taken constant for any particular pair c, c' and a, a' at constant temperature and pressure. Six types of empirical parameters are used in Pitzer's ion-interaction model with mixed electrolyte solutions. These temperature and pressure dependent parameters are $\beta_{MX}^{(0)}$, $\beta_{MX}^{(1)}$, $\beta_{MX}^{(2)}$, C_{MX}^ϕ, θ_{ij}, and Ψ_{ijk}. Using the model parameters along with solubility products, Pitzer's model can be used to predict solid solubilities in aqueous mixed-salt systems. A simplification of (A.12) for a salt solution including dissolved neutral species like gases is derived as follows. For an individual ion, an activity coefficient equation, which takes account of the neutral-ion interactions, has the following theoretical form in Pitzer's scale, where sub-index 2 refers to the dissolved gas, + to positive and – to negative ionic species, respectively.

$$\ln \gamma_+ = z_+^2 f' + m_M(2B_{MX} + ZC_{MX}) + z_+ m_M m_X C_{MX} + z_+^2 m_M m_X B_{MX}' + m_n \lambda_{nM} + \tag{A.28}$$
$$\frac{3}{2} v_- m_n (v_+ m_M + v_- m_X) \Gamma_{n,MX,MX}$$

$$\ln \gamma_- = z_-^2 f' + m_M(2B_{MX} + ZC_{MX}) + |z_-| m_M m_X C_{MX} + z_-^2 m_M m_X B_{MX}' + m_n \lambda_{nX} + \tag{A.29}$$
$$\frac{3}{2} v_+ m_n (v_+ m_M + v_- m_X) \Gamma_{n,MX,MX}$$

where

$$f' = -A_\phi \left(\frac{I^{\frac{1}{2}}}{1 + bI^{\frac{1}{2}}} + \frac{2}{b} \ln(1 + bI^{\frac{1}{2}}) \right) \tag{A.30}$$

B_{MX} and $B_{MX}^{'}$ are empirical expressions for ionic strength that are defined in a functional form, which includes the adjustable binary ion-ion interaction parameters $\beta_{MX}^{(0)}$ and $\beta_{MX}^{(1)}$. The mean activity coefficient then yields

$$v \ln \gamma_{\pm} = \left(v_+ z_+^2 + v_- z_-^2\right)f^{'} + \left(v_+ m_M + v_- m_X\right)\left(2B_{MX} + ZC_{MX}\right) + \left(v_+ z_+^2 + v_- z_-^2\right)m_M m_X B_{MX}^{'}$$
$$+ \left(v_+ z_+ + v_- z_-\right)m_M m_X C_{MX} + 2m_n\left(v_+ \lambda_{nM} + v_- \lambda_{nX}\right)$$
$$+ 3v_+ v_- m_n\left(v_+ m_M + v_- m_X\right)\left(2\tau_{n,MX} + \left|\frac{z_+}{z_-}\right|\tau_{n,MM} + \left|\frac{z_+}{z_-}\right|\tau_{n,XX}\right) \qquad (A.31)$$

The expression is simplified by defining binary and ternary parameters $\Lambda_{n,MX}$ and $\Gamma_{n,MX,MX}$, which are combined from the individual ion neutral interactions.

$$\Lambda_{n,MX} = v_+ \lambda_{nM} + v_- \lambda_{nX} \qquad (A.32)$$

$$\Gamma_{n,MX,MX} = \left(2\tau_{n,MX} + \left|\frac{z_+}{z_-}\right|\tau_{n,MM} + \left|\frac{z_+}{z_-}\right|\tau_{n,XX}\right) \qquad (A.33)$$

$$B_{MX}^{\phi} + B_{MX} = 2B_{MX} + IB_{MX}^{'} \qquad (A.34)$$

$$= 2\beta_{MX}^{(0)} + 2\beta_{MX}^{(1)}\left[\frac{2}{x^2}\left(1 - (1+x)e^{-x}\right)\right] - \beta_{MX}^{(1)}\frac{2}{x^2}\left(1 - \left(1 + x + \frac{x^2}{2}\right)e^{-x}\right)$$

$$= 2\beta_{MX}^{(0)} + \beta_{MX}^{(1)}\frac{2}{x^2}\left(1 - \left(1 + x - \frac{x^2}{2}\right)e^{-x}\right)$$

Remembering that $x = \alpha\sqrt{I}$, one yields the mean activity coefficient for an electrolyte in water:

$$\ln \gamma_{\pm} = -\left|z_+ z_-\right|A_{\phi}\left(\frac{I^{1/2}}{1 + bI^{1/2}} + \frac{2}{b}\ln(1 + bI^{1/2})\right) + m_{MX}\frac{2v_+ v_-}{v}\left(2\beta_{MX}^{(0)}\right.$$

$$+ \frac{2\beta_{MX}^{(1)}}{a^2 I}\left[1 - \left(1 + \alpha I^{1/2} - \frac{\alpha^2 I}{2}\right)\exp(-\alpha I^{1/2})\right]\right) \qquad (A.35)$$

$$+ \frac{3m_{MX}^2}{2}\left(\frac{2(v_+ v_-)^{3/2}}{v}C_{MX}^{\phi}\right) + \frac{2}{v}m_n\Lambda_{n,MX} + \frac{6v_+ v_-}{v}m_n m_{MX}\Gamma_{n,MX,MX}$$

Index n refers to neutral and MX to salt, respectively. Parameters $\beta_{MX}^{(0)}$, $\beta_{MX}^{(1)}$, C_{MX}^{ϕ} are binary ion-ion interaction parameters. These Pitzer parameters are temperature-dependent and lesser degree pressure dependent. $\Lambda_{n,MX}$ and $\Gamma_{n,MX,MX}$ parameters are temperature and lesser degree pressure dependent.